THE ASTROPHYSICAL JOURNAL, 198:383–405, 1975 June 1

GAS DYNAMICS OF SEMIDETACHED BINARIES

STEPHEN H. LUBOW AND FRANK H. SHU*
University of California, Berkeley
Received 1974 September 17

ABSTRACT

We analyze the gas dynamics of semidetached binary systems within the context of the Roche model. With the adoption of the assumptions that the contact component rotates synchronously and that the flow occurs isothermally with the thermal speed being a small fraction ϵ of the relative orbital speed, Ωd, of the two stars, we show that the steady flow can be formulated in terms of a problem with multiple length scales. Using this concept, we demonstrate the following by semianalytical methods. (1) The escape of material from the surface of the contact component is accomplished by a highly nonisotropic stellar wind which reaches sonic velocities in a neighborhood of the inner Lagrangian point, L1, of size ϵ in comparison with the orbit separation d. (2) This wind throttles into a narrow stream of material which makes a prescribed angle with respect to the line joining the stellar centers ranging from 19°.5 to 28°.4 for the full range of possible stellar mass ratios. (3) The width of the stream scales with ϵd while its density scales with $\epsilon^{-2}\dot{M}/\Omega d^3$, where $\dot{M}$ is the mass transfer rate. (4) The stream width remains nearly constant over the part of the stream which is nearly straight, and narrows somewhat as the stream curves toward the detached component. (5) If the detached component is smaller than a certain specified size, the stream results in the formation of a disk of material of prescribed size orbiting the detached component in a direct sense.

A subsidiary issue examined briefly in this paper is the flow mechanism responsible for moving material to the equator of the contact component, and from there to the L1 region where it is lost by the directed stellar wind. The mechanism of mass loss is not straightforward because the gas cannot proceed directly from high pressures to low since the strong Coriolis forces produce deflections similar to those associated with the geostrophic wind in the Earth's atmosphere.

Comparisons of our work are made with previous theoretical studies, and some applications are indicated for a variety of observed astronomical systems.

Subject headings: binaries — gas dynamics

I. INTRODUCTION

Semidetached binaries have attracted considerable astronomical interest since it was first realized that the presence of a closely orbiting companion (the detached component) may influence the evolution of a star (the contact component) once the latter has reached its Roche limit (for reviews, see Struve 1950; Kopal 1959; Paczynski 1971; Batten 1973). It has been observed that all ex-novae and U Geminorum cataclysmic variables are probably members of such close binary systems (Kraft 1963), and it has been suggested that Galactic X-ray point sources may be explained in terms of the same mass transfer model provided that the detached component of the pair is a compact object such as a neutron star or black hole (see, e.g., Giacconi 1974; Zel'dovich and Novikov 1964; Prendergast and Burbidge 1968; Pringle and Rees 1972; Lamb, Pethick, and Pines 1973; Strittmatter *et al.* 1973; Salpeter 1973; however, cf. Ostriker and Davidson 1973; and Arons 1973).

Considerable theoretical effort has been devoted to the elaboration of the mechanism of mass loss by the contact component following the suggestion by Kuiper (1941) that the Lagrangian points of the Roche model must play a central role. The approaches can be divided into two types of analyses: one using particle trajectories (see Kruszewski 1966), the other using hydrodynamical methods. The recent numerical simulation of U Cephei by Prendergast and Tamm (1974) occupies a middle ground and is perhaps the most comprehensive of the efforts to date which treat the flow beyond the inner Lagrangian point, L1.

The hydrodynamical approach would seem *a priori* to be the more applicable method (Prendergast 1960) since the mean free path in all flow regions of physical interest is many orders of magnitude smaller than the orbit separation as long as the mass transfer rate is nontrivial. Nevertheless, particle-trajectory calculations have yielded a considerable body of useful information. This fortunate circumstance arises because the effects of finite gas pressure can, to a large extent, be ignored throughout the large part of the flow that we designate the "orbit region." The argument concerning the mean free path becomes relevant here only if the ballistic trajectories try to cross one another.

One of the results of the present paper shows that the ballistic approach applies not to the motion of individual atoms but to the mean motion of the stream which leaves the surface of the contact component. Indeed, we shall confirm that the locus of the center of the gas stream can be described very accurately by purely ballistic considerations—the errors being of order ϵ^2, i.e., typically about one part in a thousand. On the other hand, a ballistic

* Alfred P. Sloan Foundation Research Fellow, 1972–1974.

description fails completely in any region of space where the effects of pressure are important. For example, without introducing hydrodynamical concepts, it is impossible to make reliable statements concerning the flow in the surface layers of the contact component, or the conditions of mass "ejection" near L1, or the width (and, therefore, the density) of the emergent stream, or the interaction of the stream with an orbiting disk.

The disadvantage of numerical hydrodynamical techniques is the enormous computing effort required on large machines (Biermann 1971; Prendergast and Taam 1974). In fact, we believe that the grid size used in such calculations is still too coarse to give reliable details because the pressure effects are important over scales which are comparable to the mesh spacing.

Our approach uses continuum mechanics and is semianalytic in the sense that most integrations can be reduced, at worst, to the numerical integration of a set of ordinary differential equations requiring a few minutes on a computer of moderate capacity. We are able to make progress because we explicitly exploit the existence of a small parameter in the problem. This parameter $\epsilon = a/\Omega d$ is the ratio of the isothermal sound speed, $a \equiv (kT/m)^{1/2}$, to the product of the angular velocity, $\Omega = 2\pi/P$, of the binary system and the separation distance d. Except for the longest period systems, ϵ has typical values of a few percent for a wide variety of physical systems ranging from Algol-type variables, cataclysmic variables, and possibly X-ray binaries. With the assumptions of synchronous rotation of the contact component and isothermal flow under steady conditions, we show that the relevant parameter space of the properly nondimensionalized and *scaled* equations reduces to a single quantity—the present mass ratio of the two stellar components. Thus, we are able to explore, with reasonable computing effort, the properties of the flow solutions for all mass transfer rates and mass ratios of physical interest (as long as $\epsilon \ll 1$) without specifying in advance the class of object under discussion until we come to the comparisons with observations.

a) Notation

In our mathematical treatment, the small parameter ϵ plays the double role of a perturbation expansion parameter for the dependent variables as well as a scale for the independent coordinate variables. To minimize confusion concerning the order of various terms, we should perhaps comment at the outset on the notation adopted. If Q represents a dependent variable whose intrinsic magnitude is, say, of order ϵ^{-1}, in a region where the coordinate q has range, say, of order ϵ, our procedure is to expand Q in the asymptotic series

$$Q = \epsilon^{-1}Q_{-1} + Q_0 + \epsilon Q_1 + \cdots ,$$

where, in general, Q_n can depend on any or all of the scaled coordinate variables

$$q_1 \equiv \epsilon^{-1}q , \qquad q_0 \equiv q , \qquad q_{-1} \equiv \epsilon q , \ldots ,$$

but Q_{-1} must depend at least on q_1.

A powerful asymptotic technique results by treating $q_1, q_0, \ldots$ as mathematically independent variables (Cole 1968; Van Dyke 1964). If ϵ is very small, one or two orders of approximation are sufficient for all practical purposes, and we can often forego the elaborate scheme of introducing several scales for the same coordinate variable, q.

b) Various Flow Regimes

Analysis of the mathematical structure of the dynamical equations reveals that the flow regimes can be separated into at least three distinct physical regions. The first region is an *orbit region* with size comparable to the separation distance of the two stars wherein the pressure effects are of order ϵ in comparison with the inertial and gravitational effects, and ballistic considerations hold to zeroth approximation. The effects of finite pressure can then be included as a small perturbation on the ballistic flow (§ IV).

The second region is the surface layer of the contact component, with scale height of order ϵ^2 compared with the orbit separation. In this layer, vertical hydrostatic equilibrium is a good approximation, but the horizontal pressure gradient drives small horizontal velocities which are, in turn, deflected by the strong Coriolis forces. The horizontal flow is, therefore, the analogue of the *geostrophic wind* of meteorology.[1] The calculation of low-speed flow patterns of stellar scale (§ V) may seem to be a futile exercise in gas dynamics inasmuch as they have little directly observable consequence; however, it is important from a physical point of view because this slow organized flow is the mechanism by which material is brought from the entire surface of the contact component to the inner Lagrangian point from which it can be "pulled out" of the star to enter the orbit region.

The third region is thus the *L1 region*, a neighborhood of the inner Lagrangian point of size ϵ compared with the separation distance, where the pressure effects are of the same order as the inertial and gravitational effects so that a full hydrodynamical treatment is necessary. This region connects the other two regions via transonic flow, and must therefore play a central role in any complete theory. A simplification is possible because this region is

[1] Prendergast (1960) introduced an approximation which he termed the "gradient wind" for his analysis of the *orbit* region. The "gradient" in his scheme refers to the gradient of the gravitational potential and not the gradient of the pressure which was taken to be zero. Thus, his scheme is physically quite distinct from the gradient-wind approximation of meteorology for which the geostrophic wind is a special case (Holton 1972; see also n. 4).

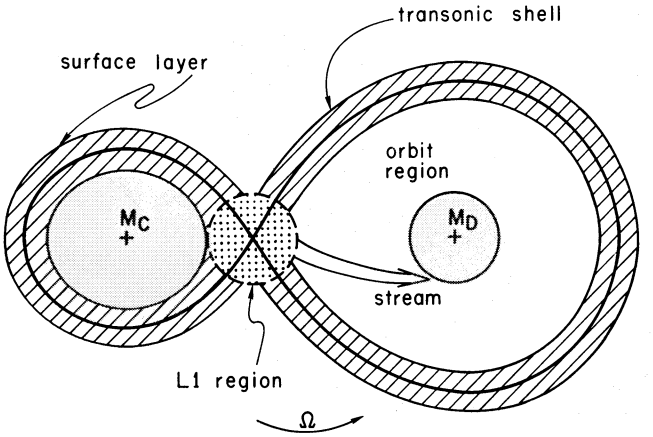

FIG. 1.—Schematic diagram of the various flow regimes in the orbit plane. The heavy curve denotes the equipotential corresponding to the Roche limit. The orbit rotation occurs in a counterclockwise sense as indicated, and the detached component is drawn in this case to be larger than the distance of minimum approach of the stream. The scales for the surface layer and the L1 region have been greatly exaggerated.

small in all three dimensions so that a truncated Taylor series expansion of the gravitational potential suffices to represent an otherwise complex gravitational field. Even so, the detailed mathematical solution of the flow in this region presents a formidable task because transonic flow involves partial differential equations of mixed type (see, e.g., Garabedian 1964, chap. 14). Fortunately, we can extract enough information about the flow in this region from general principles (§ III) to allow us to calculate many detailed features of the flow in the orbit region without needing to refer to the details of the flow near L1.

Our study of the qualitative nature of the sonic transition leads us tentatively to identify a fourth region, the *transonic* shell which corresponds to a dynamic shell of gas surrounding the Roche limit of the *detached* component. For $\epsilon \ll 1$, this region is extremely rarefied, and we have not attempted to describe it in any detail. For long-period binaries in which the contact component has an extended atmosphere, however, the transonic shell may contain more matter, and may mimic a low-density circumstellar "cloud" (cf. Batten 1973, chaps. 8 and 9). A schematic diagram of the various regimes is shown in Figure 1.

With these introductory remarks, we proceed with the formal analysis. Clearly, the sections II, III, IV, and V which follow involve quite technical discussions. The reader not concerned with these discussions may prefer to skip to § VI for a summary of the physical results and some astronomical applications.

II. FORMULATION OF THE PROBLEM

We adopt the usual Roche model to calculate the gravitational potential associated with two stars whose relative motion is a circular orbit. In a coordinate frame which rotates with the orbital motion, we regard the contact component as having "filled" its Roche lobe (in a sense to be defined more precisely later), so that the equidensity surfaces of the (very nearly) synchronously rotating surface layers correspond (very nearly) to equipotentials which pass near L1. The observational justification for this model has been reviewed by Kopal (1959).

We wish to write the gas dynamical equations in a dimensionless form. To do this, we define the unit of length to be the orbit separation d, and the unit of time to be the reciprocal of the angular speed, $\Omega^{-1} = [G(M_C + M_D)/d^3]^{-1/2}$, where M_C is the mass of the contact component and M_D the mass of the detached component. To complete our nondimensionalization, we require a characteristic density. The choice $(M_C + M_D)/d^3$ is inappropriate because it is unrelated to the densities characteristic of the *surface* layers of the contact component.

According to classical ideas, a star fills its Roche lobe when it expands to the Roche limit because of core evolution (see Paczynski 1971) or when the Roche lobe descends onto the surface of the star because of the effects of gravitational radiation (Kraft, Matthews, and Greenstein 1962; Faulkner 1972). The atmosphere of any star extends, in principle, to infinity; hence, at what point do we say that the "surface" and the Roche lobe coincide? For our problem the operational definition must be the following.

To be definite, we formulate our problem in the evolutionary context, but a simple change in wording makes our analysis applicable to mass flow driven by the decrease in orbital separation due to gravitational radiation. Thus, the slow evolutionary expansion is characterized by a small outward velocity of the outer layers. If the instantaneous mass loss rate of material being "stripped off" the layers near the Roche limit (see §§ II and V) is less than the outward mass flux crossing this equipotential surface, the star will continue to grow, with denser and denser regions being successively stripped off. Only when the density of material being stripped off is high enough that the mass loss rate is equal to the integrated outward mass flux $\dot{M}$ required by evolutionary considerations (including the instability mechanism discussed by Morton 1960) is a quasi-steady state possible.

Thus, the density of material at the surface of the contact component must be proportional to $\dot{M}$, and a proper density scale would be $\dot{M}/\Omega d^3$. Note that this choice normalizes the dimensionless mass loss rate, not the density at the surface, to unity. The surface area of the Roche lobe is of order d^2, but the outward expansional velocity is much less than Ωd, and the density in the surface layers must typically be much greater than $\dot{M}/\Omega d^3$. Indeed, we shall find the dimensional density in the general surface layers to be of order $\epsilon^{-4}\dot{M}/\Omega d^3$ while it is of order $\epsilon^{-3}\dot{M}/\Omega d^3$ in an ϵ neighborhood of L1. Moreover, since the mass transferred per orbital period is generally many orders of magnitude less than the mass of either star ($\dot{M}/\Omega \ll M_C, M_D$), we can ignore the gravity of the material in transit from M_C to M_D for its own motion.

With dimensional lengths, velocities, and densities to be recovered by multiplication, respectively, by d, Ωd, and $\dot{M}/\Omega d^3$, we can now write the steady gas dynamical equations in a corotating coordinate frame in the vector-invariant dimensionless form,

$$\nabla\cdot(\rho \boldsymbol{u}) = 0\,, \tag{1}$$

$$\nabla(\tfrac{1}{2}|\boldsymbol{u}|^2) + (\nabla \times \boldsymbol{u}) \times \boldsymbol{u} = -\frac{1}{\rho}\nabla(\epsilon^2\rho) - \nabla\phi - 2\boldsymbol{e}_Z \times \boldsymbol{u}\,. \tag{2}$$

In the above equations, we have ignored the effects of radiation pressure and we have assumed that the gas satisfies the perfect gas law so that $\epsilon^2\rho$ is the dimensionless pressure. The unit vector $\boldsymbol{e}_Z$ defines the direction normal to the orbit plane, and ϕ is the dimensionless effective potential which includes the centrifugal effects. Written in Cartesian coordinates (X, Y, Z) with $Z = 0$ defining the plane of the orbit, with the X-axis joining the line of stellar centers, and with origin at the center of mass, ϕ is given by

$$\phi = -\mu[(X - 1 + \mu)^2 + Y^2 + Z^2]^{-1/2} - (1 - \mu)[(X + \mu)^2 + Y^2 + Z^2]^{-1/2} - \tfrac{1}{2}(X^2 + Y^2)\,, \tag{3}$$

where we have introduced the standard notation

$$\mu \equiv \frac{M_D}{M_C + M_D}\,, \qquad 1 - \mu \equiv \frac{M_C}{M_C + M_D}\,. \tag{4}$$

The position of the L1 point, where $\nabla\phi = 0$ between the two stars, is given by $(X_{L1}, 0, 0)$ where X_{L1} satisfies

$$X_{L1} + \frac{\mu}{(X_{L1} - 1 + \mu)^2} - \frac{1 - \mu}{(X_{L1} + \mu)^2} = 0\,. \tag{5}$$

To close the above set of equations, we need an equation governing the variation of the temperature of the gas, i.e., an equation which determines the local value of ϵ^2. The local temperature of the gas is largely controlled by the ambient radiation field; and except for the deeper layers inside the stars, an acceptable approximation is the assumption that the gas remains isothermal throughout the flow, i.e., $\epsilon^2 = \text{constant} = kT_{\text{rad}}/(m\Omega^2 d^2)$ where T_{rad} is the "diluted" mean of the effective temperatures of the two stars and m is the mean molecular weight (assumed not to change because of changes in the ionization fraction). The isothermal assumption avoids the solution of a complex radiative transfer problem while still retaining the appropriate qualitative behavior for the calculation of the dynamics of the gas. The radiative power of the gas at the densities we are concerned with is so great that even very strong shock waves can be treated crudely as "isothermal shocks" because the width of the radiative layer where the gas cools down to the equilibrium temperature is quite thin compared with the orbit separation distance.

For $\epsilon^2 = \text{constant}$, the dot product of equation (2) with $\boldsymbol{u}$ yields Bernoulli's theorem,

$$\boldsymbol{u}\cdot\nabla(\tfrac{1}{2}|\boldsymbol{u}|^2 + \phi + \epsilon^2 \log\rho) = 0\,, \tag{6}$$

i.e.,

$$\tfrac{1}{2}|\boldsymbol{u}|^2 + \phi + \epsilon^2 \log\rho = \text{constant along a streamline}\,. \tag{7}$$

Bernoulli's theorem provides a key guiding principle in the subsequent development because it is exact to all orders in ϵ. A second important guiding principle will be the book-keeping on the mass transfer. Since star C loses mass and star D eventually gains it, we should mathematically regard the center of star C as a source of matter and the center of star D as a sink. Since the mass transfer rate is unity in the present normalization, the equation of continuity (1) should be modified to read

$$\nabla\cdot(\rho \boldsymbol{u}) = \delta(\boldsymbol{X} + \mu\boldsymbol{e}_X) - \delta[\boldsymbol{X} - (1 - \mu)\boldsymbol{e}_X]\,, \tag{8}$$

where δ is Dirac's delta function. Volume integrals of equation (8) are useful only to the extent that the left-hand side can be transformed by the divergence theorem to a surface integral well outside the deep interior of either star.

Our mathematical problem is now formulated. Given appropriate boundary conditions at infinity, on the surface of the contact component, and on the accretion surface of the detached component (which need not

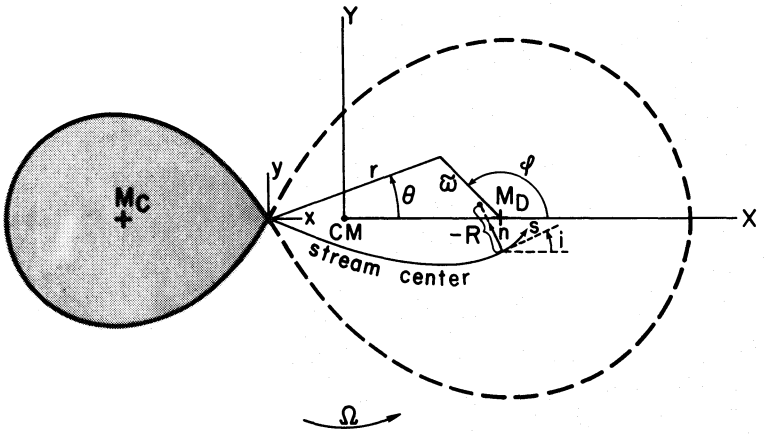

FIG. 2.—Schematic diagram of the various coordinate systems used in this paper when plotted in the orbit plane $Z = z = 0$. The symbol CM marks the center of mass of the system; and the Roche lobe of the detached component, whose center is marked with a cross, is indicated by the dashed curve. The positive z-axis points out of the plane of the paper. The quantities R and i define, respectively, the radius of curvature of the stream center and the local angle it makes with the x-direction; R is defined to be negative if the center of curvature lies in the direction of positive n.

coincide with its physical surface if it is a magnetized neutron star or a black hole), we are required to solve the partial differential equations (2) and (8) for ρ and $\boldsymbol{u}$ as a function of position. Clearly, for specified boundary conditions, the dimensionless form of the solution will depend only on two parameters, the mass ratio $\mu/(1 - \mu)$ and ϵ. If the boundary conditions possess reflection symmetry with respect to Z, it suffices to look for solutions where ρ, u_X, and u_Y are even functions of Z while u_Z is odd.

If ϵ were completely arbitrary, the complicated geometry would leave us little recourse other than numerical techniques; however, the fact that $\epsilon \ll 1$ alerts us to the possibility of using a perturbation analysis. For reasons to be discussed in the next section, this perturbation technique is asymptotic and singular in the sense of classical boundary-layer theory (see Cole 1968; Van Dyke 1964).

We shall find it convenient in what follows to use a variety of dimensionless corotating coordinate systems. These are:

1. The Cartesian coordinate system (X, Y, Z) with origin at the center of mass described earlier.
2. A Cartesian coordinate system (x, y, z) with origin at the inner Lagrangian point L1 so that $x = X - X_{L1}$, $y = Y$, $z = Z$.
3. The Roche coordinate system (ξ, η, ζ) with $\xi \equiv \phi - \phi_{L1}$ so that the surfaces of constant ξ correspond to equipotentials with $\xi = 0$ defining the Roche limit and $\xi < 0$ defining the interior of the contact component. (This differs from the definition of ξ by Kopal 1972 by the additive constant $-\phi_{L1}$.) In the very deep interior of the star, the geometry acquires spherical symmetry, and the other two coordinates, η and ζ, play the roles of the longitude and latitude. Thus, we fix the multiplicative constants by defining the ranges of η and ζ to be, respectively, $(-\pi, +\pi)$ and $(-\pi/2, +\pi/2)$ with $\zeta = 0$ defining the equatorial plane (= orbit plane for synchronous rotation), whereas the line $\zeta = -\pi/2$ points to the "north pole" (parallel to the orbit angular momentum vector $\boldsymbol{L}$, i.e., parallel to $\boldsymbol{e}_Z$), and $\zeta = +\pi/2$ points to the "south pole" (antiparallel to $\boldsymbol{L}$). On the equator the line $\eta = 0$ points toward the detached component; the L1 point corresponds, therefore, to $(\xi, \eta, \zeta) = (0, 0, 0)$. These orthogonal curvilinear coordinates have associated metric coefficients

$$h_\xi \equiv |\nabla\xi|^{-1}, \qquad h_\eta \equiv |\nabla\eta|^{-1}, \qquad h_\zeta \equiv |\nabla\zeta|^{-1}, \tag{9}$$

which have been computed numerically for a variety of cases by Kitamaru (1970).

4. Two cylindrical coordinate systems (r, θ, z) and (ϖ, φ, z) centered, respectively, on L1 and the detached component, with the positive X axis corresponding to the directions $\theta = 0$ and $\varphi = 0$.
5. The "natural" coordinates (s, n, z) for the motion of the stream; s measures the distance from L1 along the stream center, and in the plane $z = 0$, the n-direction is locally perpendicular to the length of the stream.

Except for the coordinates (ξ, η, ζ), which are plotted in Kopal (1972), these various coordinate systems are displayed in Figure 2 in the plane $z = 0$.

III. THE L1 REGION

a) General Considerations

The fact that $\epsilon \ll 1$ does not automatically allow us to ignore the pressure term in equation (2) because its gradient may be large. To illustrate this idea more concretely, consider the mechanism by which the gas escaping

from the contact component manages to attain velocities comparable to the orbit speed (unity in the present nondimensionalization). In the rotating frame, the gas must start with very small speeds on the surface of the contact component. Clearly this gas must leave the star by accelerating from subsonic speeds to supersonic speeds in a way analogous to the solar wind (Parker 1963); but in the present situation, we do not have high coronal temperatures to assist the gas in overcoming gravity.

To see where the motion can become sonic, we use the equation of continuity (1) to eliminate $\boldsymbol{u}\cdot\nabla\rho$ in equation (6), and write, with a little manipulation,[2]

$$(|\boldsymbol{u}|^2 - \epsilon^2)\nabla\cdot\boldsymbol{u} = |\boldsymbol{u}|^3\nabla\cdot\left(\frac{\boldsymbol{u}}{|\boldsymbol{u}|}\right) - \boldsymbol{u}\cdot\nabla\phi\,. \tag{10}$$

In the present context, the relevant sound speed is the isothermal sound speed ϵ. From equation (10), we see that the sonic surface where the fluid speed $|\boldsymbol{u}|$ can attain the sound speed ϵ by smooth acceleration (i.e., with $\nabla\cdot\boldsymbol{u}$ finite so that shocks are excluded), must occur where the right-hand side is equal to zero. On this surface, $|\boldsymbol{u}| = \epsilon$, while

$$\frac{\boldsymbol{u}}{|\boldsymbol{u}|}\cdot\nabla\phi = \epsilon^2\nabla\cdot\left(\frac{\boldsymbol{u}}{|\boldsymbol{u}|}\right)\cdot \tag{11}$$

Clearly, equation (11) requires that $\nabla\phi$ be small on matter-carrying streamlines. But $\nabla\phi = 0$ at L1 by definition of the L1 point, and it will be of order l in any small l neighborhood of L1. On the other hand, we expect the sonic velocity vector to change directions on a scale comparable to that in which the forces change directions, i.e., on a scale l. Thus, equation (11) implies $l = \epsilon$, and we have the very important conclusion: *The sonic point on matter-carrying streamlines must occur within an order ϵ neighborhood of the inner Lagrangian point.* This statement provides the hydrodynamical justification for the importance usually attached to the point L1.

With this knowledge, we can now make an important deduction. Since the velocities near L1 are of order ϵ and the cross-sectional area of the L1 region is of order ϵ^2, the requirement that the integrated mass flux be unity implies that *the mass density at L1 be of order ϵ^{-3} in our density units of $\dot{M}/\Omega d^3$.*

It is important to emphasize that the above conclusion applies only to matter-carrying streamtubes because the sonic surface must formally extend to very great (order unity) distances from L1. Unlike the problem of supersonic flow around solid blunt bodies, the sonic surface cannot end on the surface of the contact component since this would imply the presence of supersonic motions well inside the surface layers of the star.

Given this conclusion, we can attempt to construct the approximate location of the sonic surface at great distances from the ϵ neighborhood of L1. Clearly, the velocity vector must change directions on a scale of order unity in such regions. Equation (11) then requires that on the sonic surface the cosine of the angle between $\boldsymbol{u}$ and $\nabla\phi$ be of order ϵ^2, i.e., that the transonic flow occurs with the streamlines being very nearly parallel to equipotential surfaces. We suspect but we cannot prove that there are only two candidates for the approximate location of the sonic surfaces in these regions, namely, the two Roche lobes. The Roche lobe which contains the contact component can be eliminated immediately by the boundary condition that supersonic motions are absent in the surface layers of the contact component. We are therefore left with the Roche lobe which opens up toward the detached component.[3] We denote the dynamic shell of matter surrounding this sonic surface as the transonic shell.

This conjecture is very satisfying inasmuch as the right-hand critical surface corresponds to a "surface of zero velocity" for particles which leave L1 with zero velocity. The departure from zero velocity to sonic velocity because of finite pressure effects is associated with the fact that Bernoulli's integral (7) differs from Jacobi's integral by the addition of the heat function, $\epsilon^2 \log \rho$. All the matter from the contact component which crosses the sonic surface by smooth flow is eventually "captured" by the detached component within a volume smaller than its Roche limit. Moreover, the streamlines which cross the sonic surface at great distances (order unity) from L1 must either originate very high up in the atmosphere of the contact component or must be accompanied by very great rarefaction (see Fig. 3). Thus, the densities in the transonic shell must be very small, and all the matter-carrying streamlines must cross in an ϵ neighborhood of L1. A schematic diagram of the flow in the equatorial plane of this region is shown in Figure 3. We shall see later that this results far downstream in a narrow jet of material which virtually carries the entire mass flux away from the L1 region.

We make two comments on this point. First, Nariai (1967) has previously suggested that sonic speeds must be reached at L1 by way of analogy of the converging-diverging geometry of a de Laval nozzle. His argument is not cogent, partially because he ultimately relied on coronalike temperatures to explain the mass loss, and partially because the de Laval nozzle strictly enforces converging-diverging streamlines, i.e., $\nabla\cdot(\boldsymbol{u}/|\boldsymbol{u}|) = 0$, at the throat whereas converging-diverging equipotentials do not. In fact, the flow *must cross* equipotentials near L1 so that converging-diverging equipotentials bear little relation to converging-diverging streamlines (cf. Fig. 3); moreover,

[2] This relation has the simple generalization that the square of the effective sound speed $d(\epsilon^2\rho)/d\rho$ replaces the square of the isothermal sound speed ϵ^2 if the flow is generally barotropic rather than specifically isothermal.

[3] We are grateful to C. C. Lin for pointing out, on general principles, that it is easier for the sonic surface to open up in a direction away from the contact component than toward it.

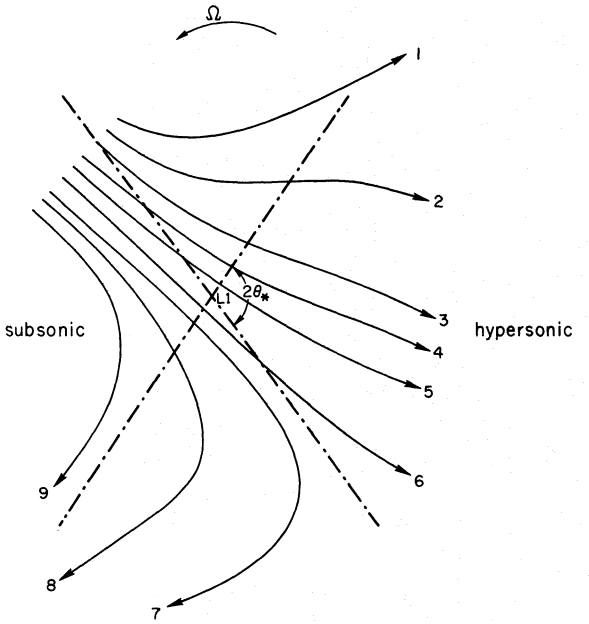

FIG. 3.—Schematic diagram of the flow in the L1 region when plotted in the orbit plane $z = 0$. The dashed-dotted lines show the equipotential curves which intersect at the point L1 at an angle $2\theta_*$. The streamline 9 lies deep in the surface layer of star C and corresponds to a very slow flow which is counter to the sense of orbit rotation in accordance with the discussion in § V. Unlike the rest of the surface layer, the gradient of the pressure is unbalanced by gravity near L1, and this leads to an outwardly directed flow for streamlines 1–8. As the fluid elements on streamlines 7 and 8 cross the Roche surface of the contact component, they must climb "uphill" against the effective potential in the bottom sector, leading to deceleration and eventual deflection by the Coriolis force back toward high pressures in the surface layers of star C. On streamlines 1–5, the fluid elements also encounter a "hill" in the top sector, but they are deflected by the Coriolis force into the "downhill" portion of the saddle-potential in the right sector, where there is little gas, leading to rapid acceleration away from the entire region. On streamline 6, only a slight "hill" is encountered, and the behavior is more similar to that of streamlines 1–5 than streamlines 7 and 8. Clearly, the material between streamlines 6 and 8 must suffer great rarefaction, whereas the material on streamline 1 is rarefied to begin with, since it originates high in the surface layer of star C. In § IIIc, we show that the material between streamlines 2 and 6 results far downstream in a narrow jet of gas which exits the L1 region with hypersonic velocities and a Gaussian density profile.

neither is needed in an absolute sense because, as in the solar wind, the transition from subsonic to supersonic flow requires only that the terms on the right-hand side of equation (10) be zero in sum, not that they be zero individually.

Second, many workers have previously speculated that "mass ejection" occurs from the contact component by "thermal evaporation" if synchronous rotation strictly applied, and have expressed skepticism that this mechanism could lead to sufficient mass loss rates (cf. Batten 1973, chap. 10). Despite the appearance of the thermal velocity, the mechanism described here is as different from thermal evaporation as a wind is different from random thermal motions. Indeed, we have reasoned in § II that a self-regulating mechanism exists whereby this wind can carry away practically any requisite amount of material demanded by the slow evolutionary expansion of the stellar "surface." A useful analogy may now be made with an inner tube being filled with air from the inside and which contains a weak spot on its outer surface. As the inner tube expands, the pressure on the weak spot bursts open a hole of fixed size through which the air rushes out. Clearly, the steady-state loss of air as well as the velocity field within the inner tube is determined only by the rate at which air is being replenished from the inside once the ambient pressure is given and the geometry of the hole is fixed. Much of the physics of the flow is contained in Bernoulli's theorem which states that the velocity is highest where the pressure is lowest (in the absence of body forces).

For our problem of semidetached binaries, the situation is more complicated, partially because the surface layers are confined by gravity and not by rubber, and partially because the presence of strong Coriolis forces does not allow a direct streaming from high pressures to low pressures on the surface of the star. We return to this question in § V, but for now we accept the contention that all the mass loss eventually occurs within an ϵ neighborhood of L1, and we turn our attention to the mathematical formulation of the equations governing the flow in this region.

b) Flow Equations in the L1 Region

We introduce the Cartesian coordinates (x, y, z) and the cylindrical coordinates (r, θ, z) which have origin at L1. Since the region of interest is small, we expand the gravitational potential in a Taylor series about L1; to

quadratic terms, this expansion has the well-known form

$$\phi = \phi_{L1} - (2A + 1)\frac{x^2}{2} + (A - 1)\frac{y^2}{2} + A\frac{z^2}{2} = \phi_{L1} - \left[1 + \frac{A}{2}(3\cos 2\theta + 1)\right]\frac{r^2}{2} + A\frac{z^2}{2}, \tag{12}$$

where A is the positive constant:

$$A \equiv \frac{\mu}{|X_{L1} - 1 + \mu|^3} + \frac{1 - \mu}{|X_{L1} + \mu|^3}. \tag{13}$$

It has values ranging from $A = 4$ for $\mu = 0$ or 1 to $A = 8$ for $\mu = \frac{1}{2}$.

We now introduce the scaled coordinates, $r_1 = \epsilon^{-1}r$ and $z_1 = \epsilon^{-1}z$, and the perturbation series, $\rho = \epsilon^{-3}\rho_{-3}(r_1, z_1) + \cdots$, and $\boldsymbol{u} = \epsilon\boldsymbol{u}_1(r_1, \theta, z_1) + \cdots$. To lowest order in ϵ, the fluid equations (1) and (2) become

$$\frac{1}{r_1}\frac{\partial}{\partial r_1}(r_1\rho_{-3}u_{r1}) + \frac{1}{r_1}\frac{\partial}{\partial\theta}(\rho_{-3}u_{\theta 1}) + \frac{\partial}{\partial z_1}(\rho_{-3}u_{z1}) = 0, \tag{14a}$$

$$u_{r1}\frac{\partial u_{r1}}{\partial r_1} + \frac{u_{\theta 1}}{r_1}\frac{\partial u_{r1}}{\partial\theta} + u_{z1}\frac{\partial u_{r1}}{\partial z_1} - \frac{u_{\theta 1}^2}{r_1} = \left[1 + \frac{A}{2}(3\cos 2\theta + 1)\right]r_1 - \frac{1}{\rho_{-3}}\frac{\partial\rho_{-3}}{\partial r_1} + 2u_{\theta 1}, \tag{14b}$$

$$\frac{u_{r1}}{r_1}\frac{\partial}{\partial r_1}(r_1u_{\theta 1}) + \frac{u_{\theta 1}}{r_1}\frac{\partial u_{\theta 1}}{\partial\theta} + u_{z1}\frac{\partial u_{\theta 1}}{\partial z_1} = -(\tfrac{3}{2}A\sin 2\theta)r_1 - \frac{1}{r_1\rho_{-3}}\frac{\partial\rho_{-3}}{\partial\theta} - 2u_{r1}, \tag{14c}$$

$$u_{r1}\frac{\partial u_{z1}}{\partial r_1} + \frac{u_{\theta 1}}{r_1}\frac{\partial u_{z1}}{\partial\theta} + u_{z1}\frac{\partial u_{z1}}{\partial z_1} = -Az_1 - \frac{1}{\rho_{-3}}\frac{\partial\rho_{-3}}{\partial z_1}. \tag{14d}$$

On this scale, the equatorial region of the surface layer is infinitely far to the left, and the orbit region is infinitely far to the right.

Physical intuition leads us to expect that hydrostatic equilibrium should prevail in the z_1-direction to the order of approximation considered here. Thus, $u_{z1} = 0$, and we can integrate equation (14d) to obtain

$$\rho_{-3}(r_1, \theta, z_1) = \rho_{-30}(r_1, \theta)\exp(-\tfrac{1}{2}Az_1^2). \tag{15}$$

The substitution of equation (15) into equations (14a)–(14c), together with the assumptions that $u_{z1} = 0$ and u_{r1} and $u_{\theta 1}$ are independent of z_1, reduces the problem to flow in two dimensions. Moreover, as $r_1 \to \infty$, the regime of hypersonic flow is the wedge, $-\theta_* < \theta < +\theta_*$, where $\pm\theta_*$ are the angles that the equipotential lines defined by $\phi = \phi_{L1}$ make with the x_1-axis in the orbit plane:

$$\cos 2\theta_* = -(2 + A)/3A, \qquad \sin 2\theta_* = 2[(2A + 1)(A - 1)]^{1/2}/3A. \tag{16}$$

As $r_1 \to \infty$ in the subsonic wedge, $\pi - \theta_* < \theta < \pi + \theta_*$, conditions of near hydrostatic equilibrium must prevail.

Equations (14a)–(14c) are to be solved subject to the integral constraints

$$\int_{\pi-\theta_*}^{\pi+\theta_*} r_1 d\theta \int_{-\infty}^{+\infty} \rho_{-3}u_{r1}dz_1 = \left(\frac{2\pi}{A}\right)^{1/2}\int_{\pi-\theta_*}^{\pi+\theta_*} \rho_{-30}u_{r1}r_1 d\theta = -1 \quad \text{as } r_1 \to \infty, \tag{17a}$$

$$\int_{-\theta_*}^{+\theta_*} r_1 d\theta \int_{-\infty}^{+\infty} \rho_{-3}u_{r1}dz_1 = \left(\frac{2\pi}{A}\right)^{1/2}\int_{-\theta_*}^{+\theta_*} \rho_{-30}u_{r1}r_1 d\theta = +1 \quad \text{as } r_1 \to \infty. \tag{17b}$$

Auxiliary boundary conditions for $r_1 \to \infty$ in the subsonic wedge are to be obtained, in principle, by matching the right-hand limit of the solution for the equatorial region of the surface layer. On the other hand, a streamline in the transonic shell which intersects the sonic surface at a very great distance from the L1 point is essentially a free streamline with zero boundary pressure. Thus, the solution of the set of equations (14) should probably be formulated in terms of the solution of a Frankl problem (see, e.g., Garabedian 1964, chaps. 12 and 14). The Cauchy problem considered by Biermann (1971) is artificial because his "initial values" are chosen arbitrarily.

c) Asymptotic Behavior of the Flow near L1

The Frankl problem posed in § III*b* is too complicated for us to pursue here. It suffices for us to consider the asymptotic behavior of the solution in the L1 region as $r_1 \to \infty$ in the two wedges of subsonic and hypersonic flow, because this behavior should be matched, respectively, by the right-hand limit of the solution of the equatorial region in the surface layer, and by the left-hand limit of the solution in the orbit region.

Clearly, as $r_1 \to \infty$ in the subsonic wedge $(\pi - \theta_*, \pi + \theta_*)$, the density distribution must approach that appropriate for hydrostatic equilibrium in all three directions, i.e.,

$$\rho_{-30}(r_1, \theta) \propto \exp\{\tfrac{1}{2}r_1^2[1 + \tfrac{1}{2}A(3\cos 2\theta + 1)]\} \quad \text{for } \pi - \theta_* < \theta < \pi + \theta_* \quad \text{as } r_1 \to \infty\,, \tag{18}$$

and the fluid velocities must approach zero consistent with the constraint (17a).

On the other hand, as $r_1 \to \infty$ in the hypersonic wedge $(-\theta_*, +\theta_*)$, $(u_{r1}^2 + u_{\theta 1}^2)$ is required to be greater than unity, and the gravitational forces in equations (14b) and (14c) must accelerate the fluid so as to produce velocities of the form

$$u_{r1} = r_1 U(\theta)\,, \qquad u_{\theta 1} = r_1 V(\theta)\,. \tag{19}$$

In this wedge, the pressure forces can play a dynamic role only if $-r_1^2\Theta(\theta)$ is the leading term in an expansion of $\log \rho_{-30}$ for large r_1. If the density is not to become exponentially small at the location of its maximum value, $\theta = \theta_s$ where $\Theta'(\theta_s) = 0$ and $\Theta''(\theta_s) > 0$, $\Theta(\theta_s)$ must itself be zero. To be compatible with equations (17b) and (19), ρ_{-30} must then be of the form

$$\rho_{-30}(r_1, \theta) = \frac{C(\theta)}{r_1} \exp\,[-r_1^2\Theta(\theta)] \tag{20}$$

in a small angular neighborhood of θ_s. In such a neighborhood, the density profile is Gaussian in θ,

$$\rho_{-30}(r_1, \theta) \approx \frac{C(\theta_s)}{r_1} \exp\left[-\frac{r_1^2}{2}\,\Theta''(\theta_s)(\theta - \theta_s)^2\right]. \tag{21}$$

Note that the density decreases as $1/r_1$ even at the center of the stream, $\theta = \theta_s$.

The above argument indicates that the flow tends to produce a narrow stream which exits the L1 region at an angle θ_s with respect to the x-axis. To determine θ_s, we substitute equations (15), (19), and (20) with $u_{z1} = 0$ into equations (14a)–(14c), and take the limit $r_1 \to \infty$. In this limit, the fluid equations become the set of ordinary differential equations

$$-2\Theta U - \frac{d\Theta}{d\theta}\,V = 0\,, \tag{22a}$$

$$U^2 + V\frac{dU}{d\theta} - V^2 = \left[1 + \frac{A}{2}\,(3\cos 2\theta + 1)\right] + 2\Theta + 2V\,, \tag{22b}$$

$$2UV + V\frac{dV}{d\theta} = -\tfrac{3}{2}A\sin 2\theta + \frac{d\Theta}{d\theta} - 2U\,. \tag{22c}$$

We now evaluate the terms in these equations at $\theta = \theta_s$. At $\theta = \theta_s$, Θ and $d\Theta/d\theta$ are zero; moreover, it is clear that the stream can exit at a constant angle θ_s independent of r_1 (as long as it is large) only if $V(\theta_s) = 0$. With these constraints, equations (22b) and (22c) provide the following conditions on θ_s and $U(\theta_s)$:

$$U^2(\theta_s) = 1 + \frac{A}{2}\,(3\cos 2\theta_s + 1)\,, \tag{23a}$$

$$U(\theta_s) = -\tfrac{3}{4}A\sin 2\theta_s\,. \tag{23b}$$

Elimination of $U(\theta_s)$ shows that *the angle θ_s that the gas stream eventually leaves the L1 region is determined only as a function of the mass ratio of the two stars and is obtained from*

$$\cos 2\theta_s = -\frac{4}{3A} + \left(1 - \frac{8}{9A}\right)^{1/2}, \qquad \sin 2\theta_s = -\left(\frac{8}{9A}\right)^{1/2}\left[1 - \frac{2}{A} + 3\left(1 - \frac{8}{9A}\right)^{1/2}\right]^{1/2}, \tag{24}$$

where the constant A is given by equation (13). We easily verify that $-\theta_* < \theta_s < +\theta_*$. The minus sign is chosen in the equation for $\sin 2\theta_s$ so that equation (23b) corresponds to outflow rather than to inflow.

We shall recover equation (24) by a much simpler analysis of the ballistic orbits in the next section. For the time being, we recall that the parameter A ranges in value only from 4 to 8 for all possible mass ratios; therefore, θ_s as given by equation (24) is a relatively insensitive function of the mass ratio. Numerical values for θ_s and other important quantities are tabulated in Table 1.

TABLE 1*

FLOW PARAMETERS IN THE L1 REGION

M_D/M_C	$X_D = 1 - \mu$	$X_C = -\mu$	X_{L1}	A	θ_s (degrees)	θ_* (degrees)	$U(\theta_s)$	$C(\theta_s)$
0.0000.....	1.0000	0.0000	1.0000	4.000	−28.37	60.00	2.508	0.2629
0.0667.....	0.9375	−0.0625	0.6859	6.162	−22.43	58.10	3.261	0.3082
0.1500.....	0.8696	−0.1304	0.5535	6.849	−21.21	57.76	3.465	0.3216
0.3000.....	0.7692	−0.2308	0.3901	7.449	−20.29	57.51	3.634	0.3329
0.5000.....	0.6667	−0.3333	0.2374	7.800	−19.81	57.38	3.730	0.3394
0.7500.....	0.5714	−0.4286	0.1010	7.964	−19.59	57.32	3.774	0.3424
1.0000.....	0.5000	−0.5000	0.0000	8.000	−19.55	57.31	3.783	0.3431
1.6667.....	0.3750	−0.6250	−0.1773	7.889	−19.69	57.35	3.754	0.3411
3.0000.....	0.2500	−0.7500	−0.3607	7.531	−20.18	57.48	3.657	0.3345
4.5000.....	0.1818	−0.8182	−0.4672	7.197	−20.66	57.61	3.564	0.3282
5.5000.....	0.1538	−0.8462	−0.5132	7.020	−20.94	57.68	3.514	0.3249
7.0000.....	0.1250	−0.8750	−0.5631	6.805	−21.28	57.77	3.453	0.3208
8.5000.....	0.1053	−0.8947	−0.5991	6.634	−21.57	57.86	3.403	0.3175
10.0000.....	0.0909	−0.9091	−0.6266	6.494	−21.82	57.92	3.361	0.3147
15.0000.....	0.0625	−0.9375	−0.6859	6.162	−22.43	58.10	3.261	0.3082
∞.....	0.0000	−1.0000	−1.0000	4.000	−28.37	60.00	2.508	0.2629

* Note the symmetry with respect to the interchange of μ and $1 - \mu$; for example, compare the entries for $M_D/M_C = 0.0667 = 1/15$ and $M_D/M_C = 15$.

It is now possible to develop a series solution of equations (22) in the form

$$\Theta = \tfrac{1}{2}[U^2(\theta_s) - A + 2](\theta - \theta_s)^2 + \cdots , \tag{25a}$$

$$U = U(\theta_s) + 2(\theta - \theta_s) + \cdots , \tag{25b}$$

$$V = -U(\theta_s)(\theta - \theta_s) + \cdots . \tag{25c}$$

For θ near θ_s, the vector addition of the velocities implied by equations (25b) and (25c) leads to parallel flow with a uniform shear across the stream $r_1^{-1}\partial u_{r1}/\partial\theta = 2$. This result has a simple interpretation in terms of Kelvin's circulation theorem (see § IV*d*).

Since $U(\theta)$, $C(\theta)$, and $\Theta(\theta)$ are smoothly varying functions in the neighborhood of $\theta = \theta_s$, the integration of equation (17b) can be performed by the usual method of steepest descent. This shows the coefficient $C(\theta_s)$ which enters in equation (21) to be given as

$$C(\theta_s) = \frac{\{A[U^2(\theta_s) - A + 2]\}^{1/2}}{2\pi U(\theta_s)} . \tag{26}$$

The above result completes our formal derivation of the properties of the flow in the L1 region.

Since supersonic flow is often formulated in terms of an initial-value problem, it may seem paradoxical that we have been able to deduce the far downstream properties of the flow without reference to the detailed conditions which prevail near the sonic surface. Our understanding of this result depends on the explicit recognition of the crucial role played by the linear increase with r_1 of the body forces in shaping the eventual downstream characteristics of the stream. An analogy may be made with a harmonic oscillator which is forced at ever increasing amplitude. Clearly, as t becomes large, the effects introduced by the initial conditions become negligible in comparison to the forced response. Frictional damping of transients would only reinforce this conclusion.

IV. THE ORBIT REGION

a) Reduction to Two Dimensions

We have seen that the flow out of the L1 region toward the orbit region becomes two-dimensional because hydrostatic equilibrium tends to be maintained in the z-direction, and the gas becomes confined to a thin layer in the orbit plane. Strict hydrostatic equilibrium will not prevail in the orbit region because the z-component of the gravity varies with horizontal position; nevertheless, it is a useful approximation to eliminate the uninteresting dimension of the flow. To reduce the flow problem to one involving only the two interesting dimensions, we follow the procedure used in the investigation of the dynamics of thin galactic disks.

We write the full gas dynamical equations expressed in Cartesian coordinates in their conservation (divergence) forms, and we approximate the solution to the z-component of the momentum equation by the hydrostatic solution,

$$\rho = \rho^{(0)} \exp\,[-\epsilon^{-2}(\phi - \phi^{(0)})] \quad \text{with } \phi - \phi^{(0)} \approx \tfrac{1}{2}\omega_z^2 z^2 , \tag{27}$$

where the superscript zero denotes a quantity is to be evaluated at $z = 0$ and where for small z we can replace $\phi - \phi^{(0)}$ by its truncated Taylor series, $\omega_z^2 z^2/2$, with $\omega_z^2 \equiv (\partial^2\phi/\partial z^2)_{z=0}$ being the square of the z-oscillation frequency. We define the surface density

$$\sigma \equiv \int_{-\infty}^{+\infty} \rho dz \approx \epsilon \frac{(2\pi)^{1/2}}{\omega_z} \rho^{(0)}(x, y) , \tag{28}$$

and the variation of the z-component of gravity is now reflected in the horizontal variation of $\omega_z(x, y)$.

We expect ϕ, u_x, u_y to be slowly varying even functions of z, and ρu_z to vanish as $|z| \to \infty$. If we substitute the expression (27) into the gas dynamical equations written in their conservation forms and use the method of steepest descent to perform integrations over all z, we obtain

$$\frac{\partial}{\partial x}(\sigma u_x^{(0)}) + \frac{\partial}{\partial y}(\sigma u_y^{(0)}) = 0 , \tag{29a}$$

$$\frac{\partial}{\partial x}(\sigma u_x^{(0)} u_x^{(0)}) + \frac{\partial}{\partial y}(\sigma u_x^{(0)} u_y^{(0)}) = -\epsilon^2 \frac{\partial \sigma}{\partial x} - \sigma \frac{\partial \phi^{(0)}}{\partial x} + 2\sigma u_y^{(0)} , \tag{29b}$$

$$\frac{\partial}{\partial x}(\sigma u_y^{(0)} u_x^{(0)}) + \frac{\partial}{\partial y}(\sigma u_y^{(0)} u_y^{(0)}) = -\epsilon^2 \frac{\partial \sigma}{\partial y} - \sigma \frac{\partial \phi^{(0)}}{\partial y} - 2\sigma u_x^{(0)} . \tag{29c}$$

Although equations (29) are approximate relations, we can adopt them as exact *model* equations for the purpose of expansion in powers of ϵ. Thus, we can drop the cumbersome superscript zero notation, and we can write equations (29) in the equivalent vector invariant forms

$$\nabla \cdot (\sigma \boldsymbol{u}) = 0 , \tag{30a}$$

$$\nabla B + (2\boldsymbol{e}_z + \nabla \times \boldsymbol{u}) \times \boldsymbol{u} = 0 , \tag{30b}$$

where B is the two-dimensional form of Bernoulli's integral

$$B \equiv \tfrac{1}{2}|\boldsymbol{u}|^2 + \phi + \epsilon^2 \log \sigma = \text{constant along a streamline without shocks} , \tag{31}$$

and where ∇ is interpreted in equations (30) as the two-dimensional "del operator" with $\boldsymbol{u}$ and ϕ to be evaluated in the plane $z = 0$. Note that the curl of equation (30b) recovers Kelvin's circulation theorem in a form appropriate for steady barotropic flow in a rotating frame of reference. Its three-dimensional analog can, of course, be obtained by taking the curl of equation (2).

b) Ballistic Trajectories

In the orbit region, the natural length scale for the variation of $\boldsymbol{u}$ and ϕ is unity, whereas $\log \sigma$ varies on a length scale ϵ (see § IV*d*). Thus, the pressure effects are everywhere negligible in the zeroth order of approximation, and upon substitution of the perturbation series $\boldsymbol{u}(\boldsymbol{x}) = \boldsymbol{u}_0(\boldsymbol{x}) + \epsilon \boldsymbol{u}_1 + \cdots$ into equation (30b), we obtain to lowest order

$$u_{x0} \frac{\partial u_{x0}}{\partial x} + u_{y0} \frac{\partial u_{x0}}{\partial y} = -\frac{\partial \phi}{\partial x} + 2u_{y0} , \tag{32a}$$

$$u_{x0} \frac{\partial u_{y0}}{\partial x} + u_{y0} \frac{\partial u_{y0}}{\partial y} = -\frac{\partial \phi}{\partial y} - 2u_{x0} . \tag{32b}$$

We shall consider the equation of continuity (30a) later when we discuss the next-order approximation, but for the present we note that the quasi-linear partial differential equations (32) form a complete set to solve for u_{x0} and u_{y0}. In particular, the characteristic equations associated with this set,

$$\frac{du_{x0}}{dt} = -\frac{\partial \phi}{\partial x} + 2u_{y0} , \quad \frac{du_{y0}}{dt} = -\frac{\partial \phi}{\partial y} - 2u_{x0} , \quad \text{on the curve} \quad \frac{dx}{dt} = u_{x0} , \quad \frac{dy}{dt} = u_{y0} , \tag{33}$$

are equivalent to the ballistic trajectories of free particles.

Only a very restricted class of ballistic trajectories, however, is relevant to our present problem because we require that the streamlines not cross each other, and that they originate from an ϵ neighborhood of L1 with velocities of magnitude ϵ. In the spirit of matched asymptotic expansions, therefore, we require in the limit that ϵ can be considered to be arbitrarily small, that the left-hand limit of the ballistic trajectories satisfy the conditions

$$u_{x0} \to 0 , \quad u_{y0} \to 0 , \quad \text{as } x, y \to 0 \quad \text{(i.e., as } \boldsymbol{X} \to \text{L1)} . \tag{34}$$

For small x and y, the substitution of the Taylor series expansion (12) yields the orbit equations (33) in the form

$$\ddot{x} = (2A + 1)x + 2\dot{y} , \quad \ddot{y} = -(A - 1)y - 2\dot{x} . \tag{35}$$

These equations are standard in the stability analysis of celestial mechanics for the equilibrium at the L1 point (see, e.g., Moulton 1914 or Szebehely 1967). The general solution of the linear set (35) is well known and can be expressed in the real form

$$x = a_1 \sinh \lambda_1 t + a_2 \cosh \lambda_1 t + a_3 \sin \lambda_3 t + a_4 \cos \lambda_3 t\,, \tag{36a}$$

$$y = m_1 a_1 \cosh \lambda_1 t + m_1 a_2 \sinh \lambda_1 t + m_3 a_3 \cos \lambda_3 t - m_3 a_4 \sin \lambda_3 t\,, \tag{36b}$$

$$\lambda_1 \equiv \{\tfrac{1}{2}[(A-2) + (9A^2 - 8A)^{1/2}]\}^{1/2}\,, \qquad \lambda_3 \equiv \{\tfrac{1}{2}[-(A-2) + (9A^2 - 8A)^{1/2}]\}^{1/2}\,, \tag{36c}$$

$$m_1 \equiv \frac{\lambda_1^2 - (2A+1)}{2\lambda_1}\,, \qquad m_3 \equiv \frac{\lambda_3^2 + (2A+1)}{2\lambda_3}\,. \tag{36d}$$

The orbit time t in equations (36a) and (36b) gives the solution for the fluid velocities $u_{x0} = \dot{x}$ and $u_{y0} = \dot{y}$ in parametric form; it is to be eliminated if we wish to recover u_{x0} and u_{y0} as functions of x and y (the "Eulerian" description).

The only form of equations (36a) and (36b) which can satisfy the conditions (34) are the "straight line" solutions, $a_1 = a_2 \equiv a > 0$ with a arbitrary, and $a_3 = a_4 = 0$:

$$x = a \exp(\lambda_1 t)\,, \qquad y = m_1 a \exp(\lambda_1 t)\,. \tag{37}$$

Thus, on the order unity scale, the fluid element is at L1 at $t = -\infty$, and it takes "infinite" time for it to leave from L1. The geometric form of the streamline in the left-hand limit of the orbit region is given by the straight line

$$y/x = m_1 = \text{constant} < 0\,. \tag{38}$$

Some straightforward trigonometric substitutions show that m_1 is equivalent to $\tan(\theta_s)$, where θ_s is the angle defined by equation (24). Moreover, along the straight portion of the stream, the fluid velocities increase linearly with distance along the streamline (38):

$$u_{x0} = \lambda_1 a \exp(\lambda_1 t)\,, \qquad u_{y0} = m_1 \lambda_1 a \exp(\lambda_1 t)\,. \tag{39}$$

Thus, the left-hand limit of the flow in the orbit region corresponds in the lowest order of approximation to an (infinitely) narrow stream leaving L1 with the same characteristic angle and velocity field as the right-hand limit of the flow in the L1 region.

The present derivation sheds light on the physical mechanism which produces this straight-line behavior. When the gas tries to stream out of the L1 region, the effect of the Coriolis force (i.e., the tendency to conserve angular momentum in an inertial frame of reference) is to make it turn in a retrograde sense with respect to the orbital motion of the two stars. On the other hand, the effect of the gravitational pull of the detached component is to turn the stream in a direct sense when it tries to move downward in the (x, y)-plane. The balance of these two tendencies in the direction normal to the actual path produces a straight line near L1. Of course, the effective gravity in the direction parallel to the stream is unbalanced, and this produces a continuous acceleration of the stream with an acceleration per unit length equal to $\lambda_1 = U(\theta_s)$.

From purely a particle-orbit point of view, the result (37) is more general than its derivation. One could argue that all the particles start with positions near L1 and with small initial velocities, and, thus, all the coefficients $\{a_i\}_{i=1}^4$, in equations (36a) and (36b) are comparably small if we take the initial instant to be $t = 0$. (In contrast, the coefficient a which appears in eq. [37] is of order unity because we put the initial instant at $t = -\infty$.) The asymptotic limit of all such orbits as t becomes large is, then, the straight-line solution: $x = \frac{1}{2}(a_1 + a_2) \exp(\lambda_1 t)$ and $y = \frac{1}{2} m_1 (a_1 + a_2) \exp(\lambda_1 t)$. Almost exactly this derivation was presented by Kuiper (1941) to explain the asymptotic straight-line behavior of numerically computed orbits of particles ejected from L1 with low speeds (cf. Warner and Peters 1972).

From a technical point of view, however, the second argument is inferior to the first because only orbit (37) should be used to follow *fluid elements* out of L1. The practical advantage in using the expression (37) as the starting condition for the numerical integration of the full orbit is that we do not waste computing time following trajectories (which intersect) out of a small region of space near L1 where the particle-trajectory approach precisely does not apply.

Figure 4*a* shows the numerical continuation of the trajectory of the stream center. The salient qualitative feature of Figure 4*a* is the tendency for the stream to continue on a nearly straight-line path even well past the neighborhood of L1. The numerical accuracy of these computations to a few parts in 10^4 was verified by checking the constancy of Jacobi's integral.

c) Disk Formation

How far does the orbit solution extend? Clearly, if the detached component were large enough, it would intercept the stream at some point on its ballistic trajectory, and our problem would come to an end, apart from a separate

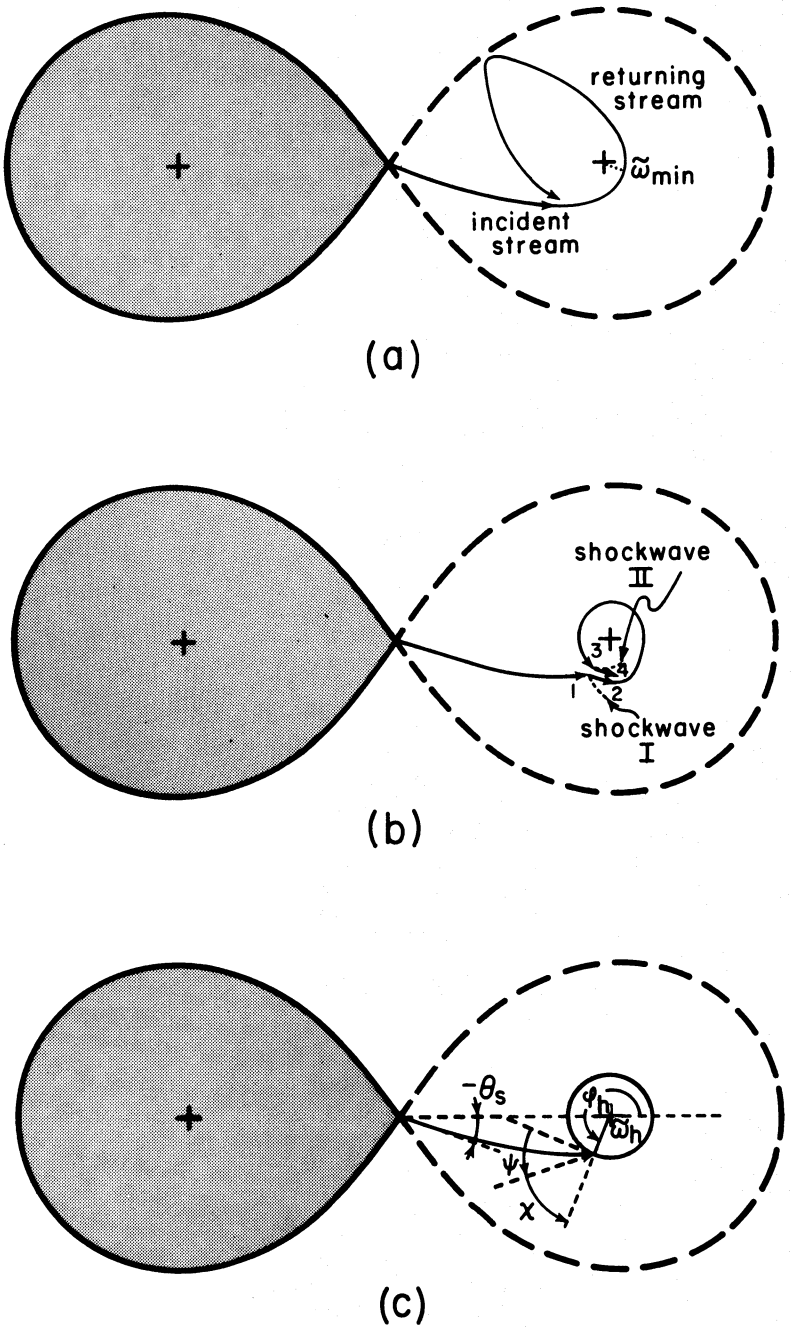

FIG. 4.—Stream trajectory and disk formation in the orbit plane graphed for the case of equal masses. (*a*) The stream which leaves L1 returns to strike itself after having reached a minimum distance, ϖ_{min}, without having been intercepted by the surface of the detached component. Note that the stream trajectory does not extend beyond the Roche lobe of the detached component. (*b*) Schematic interaction of the stream with the disk edge in the steady-state flow. The interactions of the outermost stream segments at the disk edge are described in the text; in the interior of the disk, the material spirals slowly in toward the detached component. The accretion mechanism operating in the disk interior is not discussed in detail in this paper. (*c*) Geometry for stream-disk interaction for the steady-state configuration. The disk edge corresponds to a simple periodic orbit, and at the point of impact (ϖ_h, φ_h), $|u_{\text{stream}}| \cos \psi = |u_{\text{disk edge}}|$. The average radius of the disk edge, ϖ_d, is empirically determined to give a good approximation for ϖ_h.

study of the gas dynamics and radiation field produced in the "hot spot" of such a high-velocity impact. If the detached component is smaller than the minimum distance of approach of the stream to the center of the star $\varpi_{\min}$, the situation is more complicated.

To analyze the steady-state resolution of such a situation, we perform the following gedankenexperiment. Imagine an initial stream of material which leaves L1. If the radius of the detached component is smaller than the distance of closest approach, $\varpi_{\min}$, the stream would not strike the surface of the companion star, but would proceed to orbit asymmetrically around the star eventually to strike itself (see Fig. 4*a*). The action of the returning stream striking the incident stream is to produce two strong radiating shocks which deflect the subsequent path of the incoming stream downward in the (x, y)-plane and the returning stream rightward. This impact does not affect the prior trajectory of the incoming stream because no disturbance can propagate upstream in supersonic flow, but the downstream flow is altered drastically. The subsequent transient behavior (which may last for hundreds to thousands of orbital periods) is complicated because each new impact produces new deflections which alter the downstream flow. Fortunately, the steady-state resolution is simple. If we ignore for the moment any motions in the z-direction, the steady-state geometry should correspond to the situation depicted in Figure 4*b*.

The incident stream segment 1 is deflected by its returning segment 3 into segment 2 while the returning segment 3 is deflected by the incoming segment 1 into segment 4 which travels parallel to segment 2. Inside these interacting streams may lie a disk of material left over from previous interactions, and segments 3 and 4 are properly regarded as the outer edge of that disk.

We shall assume that segment 2 flows into segment 3 without the production of shocks, and we shall now see that this is equivalent to the assumption of a large contrast in densities between the disk and the incident stream. Such a large contrast in densities results because the material in the disk must lose most of its angular momentum with respect to the detached component before it can be accreted by the latter, and the mechanism of angular momentum transport is unlikely to be efficient. We return to this question later, but for the present we concentrate on the interaction of the outermost streams.

In a steady state, the velocity of segment 4 must not differ greatly from the velocity of segment 2; otherwise, the large slip across the two streams would result in a very strong Kelvin-Helmholtz instability (see, e.g., Chandrasekhar 1961) which would quickly mix the two streams and reduce the slip. On the other hand, segment 3 is just the smooth-flow continuation of segment 2 for which Bernoulli's theorem (31) applies. Segments 1, 2, 3, and 4 have nearly the same positions in space if we assume that the cooling regions behind the radiating shocks are thin; therefore, the term ϕ which enters in Bernoulli's integral has very nearly the same value in segments 2 and 3. Since the term $\epsilon^2 \log \sigma$ is small because of the multiplicative factor ϵ^2, Bernoulli's theorem now requires that the speeds of segments 2 and 3 be nearly equal. But we have already reasoned that segments 2 and 4 have nearly equal velocities if strong instabilities are to be avoided. Thus, segments 3 and 4 must have nearly the same speeds (differing by amounts comparable to the sound speed), and unlike the shock wave I which deflects segment 1 into segment 2, the shock wave II which deflects segment 3 into segment 4 cannot be very strong. This can be the case only if the density of the disk edge is much greater than that of stream segment 1. (Q.E.D.) Stream segment 1 effectively slams into a "solid wall" and is deflected by a strong radiating shock to turn parallel to the wall. The disk edge is not really solid, but it suffers relatively little deflection because of the large contrast in densities.

Given the above picture, it is now an easy matter to calculate the size and the shape of the outer edge of the disk. To a good first approximation, the motion from point 2 to 3 to 4 in Figure 4*b* constitutes a simple periodic orbit of family g or i in the terminology of the Copenhagen school of celestial mechanics (Strömgren 1935). These direct orbits can be constructed numerically for a wide range of sizes by standard techniques. The simple periodic orbit which corresponds to the outer edge of the disk can then be found by the following criterion: *The velocity component of the incident stream resolved in the tangential direction of the simple periodic orbit at the point of their intersection must equal the speed of the simple periodic orbit at that point* (Fig. 4*c*).

When we carried out this program numerically, we discovered empirically that the size of the disk edge is usually a small fraction (typically about 0.1) of the stellar separation. The simple periodic orbits in this situation are close to being circles because of their proximity to the detached component. An acceptable time-saving procedure exists since the average radius of the orbit, ϖ_d, can be regarded as a small perturbation parameter. (This technique differs somewhat from that of Huang 1967 wherein M_C is assumed to be $\ll M_D$.) Our perturbation analysis, which we do not reproduce here for lack of space, shows that the Jacobi integral per unit mass, H, associated with the simple periodic orbit can be expanded as the following series in the angle-averaged radius ϖ_d:

$$H = -\tfrac{1}{2}(1-\mu)(3-\mu) - \frac{\mu}{2\varpi_d}\left[1 + \varpi_d^{3/2}\frac{2}{\mu^{1/2}} + \varpi_d^{3}\left(\frac{1-\mu}{\mu}\right) + \cdots\right]. \tag{40}$$

To the same order, the angle-averaged value of the angular momentum per unit mass, with respect to the detached component in the rotating frame, reads

$$\langle J\rangle \equiv \langle \varpi^2\dot{\varphi}\rangle = (\mu\varpi_d)^{1/2}\left[1 - \frac{\varpi_d^{3/2}}{\mu^{1/2}} - \frac{\varpi_d^{3}}{4}\left(\frac{1-\mu}{\mu}\right) + \cdots\right]. \tag{41}$$

TABLE 2

PARAMETERS FOR DISK FORMATION

M_D/M_C	$\varpi_{\min}$	ϖ_d	$\varphi_h - 180°$ (degrees)	χ (degrees)	$\lvert u\rvert$	u_φ	u_ϖ
0.0667	0.0228	0.0404	73.86	51.32	1.541	1.203	−0.963
0.1500	0.0276	0.0492	73.46	51.04	2.030	1.578	−1.276
0.3000	0.0329	0.0589	72.78	50.91	2.475	1.921	−1.560
0.5000	0.0382	0.0683	71.93	50.96	2.756	2.141	−1.736
0.7500	0.0438	0.0780	70.95	51.12	2.910	2.266	−1.827
1.0000	0.0488	0.0865	70.05	51.31	2.968	2.317	−1.856
1.6667	0.0604	0.1058	68.00	51.82	2.956	2.324	−1.827
3.0000	0.0793	0.1363	64.86	52.69	2.777	2.209	−1.683
4.5000	0.0966	0.1631	62.21	53.45	2.585	2.076	−1.539
5.5000	0.1066	0.1781	60.76	53.87	2.477	2.001	−1.461
7.0000	0.1198	0.1978	58.92	54.40	2.343	1.905	−1.364
8.5000	0.1316	0.2147	57.37	54.85	2.233	1.826	−1.286
10.0000	0.1422	0.2297	56.02	55.23	2.141	1.759	−1.221
15.0000	0.1714	0.2698	52.52	56.20	1.918	1.594	−1.067

These expressions become exact expressions in the limit $\mu \to 1$. For $\mu < 1$, the radius of impact, ϖ_h, differs fractionally from ϖ_d only by a term of order $\varpi_d{}^3$.

If we now replace the actual simple periodic orbit by an "equivalent circular orbit" whose properties are described by equations (40) and (41), our criterion for the determination of the disk edge becomes that the φ-component of the incident stream velocity should equal $\langle J\rangle/\varpi_d$. In this approximation, $\psi + \chi = 90°$. Tabulated in Table 2 are the values of ϖ_d determined this way as well as other parameters of geometric interest for a variety of mass ratios. The symbols for the various tabulated quantities correspond to those given in Figure 4*c*. The error in the determination of ϖ_d by using the "equivalent circular orbit" rather than the exact simple periodic orbit has been estimated to be less than about 0.1 percent for the entries in this table.

Previous determinations of the size of the disk, based on particle trajectory calculations, have been given by Kruszewski (1967) and by Warner and Peters (1972) under the assumption that the angular momentum per unit mass of an unperturbed circular orbit about the detached component is equal to that of the stream. This algorithm is logically ad hoc, but the fortunate combination of a large density contrast and a small value of ϖ_d makes their procedure formally equivalent to ours if we were simply to retain only the first term in the expansion (41).

Direct comparisons between our results and Kruszewski's are not possible because he concentrated on the role of nonsynchronous rotation. In any case, the values of ϖ_d computed by us do not show the upper limit 0.17 found in his work.

Warner and Peters (1972) considered the case of synchronous rotation. A comparison of their Table 1 and our Table 2 shows discrepancies which are too large to be attributed to the number of terms retained in equation (41); in fact, the discrepancies become worse if we retain only the first term. Their stream orbit calculations are nearly in exact agreement with ours; a simple physical argument shows that a program error must reside in their angular-momentum matching algorithm. This argument also lends some physical insight into the dynamics.

The angle χ in Figure 4*c* must be larger than 45° because the stream speed at the point of impact cannot exceed that of the disk edge by more than a factor of $\sqrt{2}$. This results because the effects of the contact component and of being in a rotating frame of reference are small for $\varpi_d \ll 1$, and a particle falling from rest at L1 can clearly only reach smaller speeds than a particle falling from infinity. Thus, the tangential velocity component of the incident stream can equal the "equivalent circular speed" only if χ is greater than 45°. Our values of χ are always somewhat greater than 45°, but those tabulated by Warner and Peters are not.

We now turn our attention to another theoretical point of some current interest. Various workers (see, e.g., Burbidge and Prendergast 1968; Pringle and Rees 1972) have commented on the possible role of turbulent transfer of angular momentum for the problem of mass accretion in a rotating disk. The angular momentum obstacle is very real even in our picture because the angular momentum of a fluid element traveling in a simple periodic orbit is conserved over one period even if it is not for all times.

We remark, however, that if the disk is turbulent, it must be driven so; it does not become so because of any intrinsic instability associated with the differential rotation. Suppose an accretion disk could be induced to form without *any* transfer of angular momentum; then the laminar flow in the disk would be marginally stable by Rayleigh's criterion because the angular momentum per unit mass in an inertial frame would be constant as a function of its radius. If, as is more likely, each fluid element loses some angular momentum as it is forced to move inward, the laminar flow is stable by Rayleigh's criterion because the angular momentum per unit mass would then *increase outward*. The theoretical analysis and laboratory experiments conducted by G. I. Taylor on Couette flow between concentric cylinders indicates that the laminar flow is then stable at *all* Reynolds numbers (see Lin 1955, chaps. 2 and 4).

Some turbulence can undoubtedly be driven in the neighborhood of the impact of the stream with the disk. First, we have already remarked that a lack of "synchronization" between the tangential velocity components of the stream and the disk edge results formally in a tangential discontinuity which would in reality broaden into a turbulent region. We believe this mechanism to be responsible for keeping the disk at its computed size. If the disk radius ϖ is smaller than the value ϖ_d, the addition of fresh stream material "spins up" the disk until $\varpi = \varpi_d$, and vice versa. Moreover, even if the stream center satisfies a condition of zero slip, some turbulence would result because the vorticity in stream segment 1 (see eq. [59]), even after modification by passage through the curved shock wave I, would generally be incompatible with the vorticity required for Keplerian motion.

Second, the normal component of the stream's impact velocity would not decelerate virtually to zero at distances in z which are much greater than the scale height of the disk. The material behind the bow shock in these regions must "spill over" the top and bottom of the disk in a manner similar to supersonic flow past blunt bodies. The large slip velocities present in the boundary layers are likely to lead to a turbulent wake whose largest eddies have sizes comparable to the disk thickness.

These local sources of turbulence have associated time scales which are comparable to the "flickering" observed in the light curves of some close binary systems, but it is doubtful that they can be substantially convected into the interior of a *dense* disk. If magnetic fields play a role in the vertical balance of the differentially rotating disk, the Parker instability (see, e.g., Shu 1974) may be a more important source of turbulence in the interior regions of the disk. In any case, the turbulence induced in the disk can hardly be very supersonic, and we do not expect it to affect our considerations of the disk size or shape since the mean flow involves hypersonic velocities.

Our personal preference for the angular-momentum transfer mechanism involves the presence of weak shock wave structures throughout the disk. Large-scale shock waves in the presence of gravitating bodies are known to be capable of making rotating elements of gas in spiral galaxies lose angular momentum (Roberts and Shu 1972), and related mechanisms may work here. To be sure, the physical environments are entirely different, and we shall not pursue the analogy further in the present paper.

d) Stream Spreading

The zeroth-order calculation (ballistic trajectory) cannot give any information concerning the width of the actual stream in the orbit region. To discuss this problem, we need to consider the next-order equations.

Our analysis begins with the adoption of the "natural coordinates" (s, n), where s is the distance from L1 measured along the zero-order trajectory, and n is the normal to this direction defined so that $\boldsymbol{e}_s \times \boldsymbol{e}_n = \boldsymbol{e}_z$ (see Fig. 1). The curve $n = 0$ (ballistic trajectory) is given parametrically in (x, y)-coordinates in the form

$$x = x_0(t), \qquad y = y_0(t). \tag{42}$$

The radius of curvature R of this curve, defined to be negative if $\boldsymbol{e}_n$ points toward the center of curvature, is given by

$$R = \frac{(\dot{x}_0^2 + \dot{y}_0^2)^{3/2}}{\dot{y}_0\ddot{x}_0 - \dot{x}_0\ddot{y}_0}, \tag{43}$$

and can be expressed implicitly as a function of s once we integrate the equation

$$\frac{ds}{dt} = (\dot{x}_0^2 + \dot{y}_0^2)^{1/2} \tag{44}$$

subject to the initial condition $s = 0$ at L1. The displacement vector from (s, n) to $(s + ds, n + dn)$ has the form $\boldsymbol{e}_s(R + n)ds/R + \boldsymbol{e}_n dn$; hence, the metric coefficients for the (s, n) curvilinear coordinates are

$$h_s = 1 + \frac{n}{R(s)}, \qquad h_n = 1. \tag{45}$$

The transformation $(x, y) \rightarrow (s, n)$ can now be completed with the aid of the formulae

$$x = x_0(s) - n \sin i(s), \qquad y = y_0(s) + n \cos i(s), \tag{46}$$

where $i(s)$ can be found from the formula $\tan i = y_0'(s)/x_0'(s)$, or from the differential equation

$$\frac{di}{ds} = -\frac{1}{R(s)} \qquad \text{with} \qquad i = \theta_s \qquad \text{at} \qquad s = 0. \tag{47}$$

We state without proof that the radius of curvature R has a finite value at L1. It can be found by carrying a series expansion of the orbit equations to one higher order in x_0 and y_0 than that considered in § IV*b*.

In the (s, n) coordinate system (single-valued for $|n| \ll R$), the fluid equations (30) can be written as

$$\left(\frac{R}{R+n}\right)\frac{\partial}{\partial s}(\sigma u_s) + \frac{\partial}{\partial n}(\sigma u_n) + \frac{\sigma u_n}{R+n} = 0\,, \tag{48a}$$

$$\left(\frac{R}{R+n}\right)u_s\frac{\partial u_s}{\partial s} + u_n\frac{\partial u_s}{\partial n} + \frac{u_n u_s}{R+n} = -\left(\frac{R}{R+n}\right)\left(\frac{\partial\phi}{\partial s} + \frac{\epsilon^2}{\sigma}\frac{\partial\sigma}{\partial s}\right) + 2u_n\,, \tag{48b}$$

$$\left(\frac{R}{R+n}\right)u_s\frac{\partial u_n}{\partial s} + u_n\frac{\partial u_n}{\partial n} - \frac{u_s^2}{R+n} = -\left(\frac{\partial\phi}{\partial n} + \frac{\epsilon^2}{\sigma}\frac{\partial\sigma}{\partial n}\right) - 2u_s\,, \tag{48c}$$

where the partial derivatives of ϕ with respect to s and n can be obtained from their counterparts in x and y by using the transformation formulae (46). We wish to solve equations (48) subject to the integral constraint

$$\int_{\text{stream width}} \sigma u_s dn = 1\,, \tag{49}$$

and subject to the boundary conditions that the solutions match the right-hand asymptotic behavior of the L1 region solution.

From our discussion of § III, we expect the stream to be very narrow (width of order ϵ); hence, we are motivated to introduce the length scale

$$n_1 = \epsilon^{-1}n\,. \tag{50}$$

We now expand the gravitational potential and field in a Taylor series expansion about the center of the stream, $n = 0$,

$$\phi = \phi_0(s) + \epsilon n_1\left(\frac{\partial\phi}{\partial n}\right)_0 + \tfrac{1}{2}\epsilon^2 n_1^2\left(\frac{\partial^2\phi}{\partial n^2}\right)_0 + \cdots\,, \tag{51a}$$

$$-\frac{1}{h_s}\frac{\partial\phi}{\partial s} = -\left(\frac{\partial\phi}{\partial s}\right)_0 + \epsilon n_1\left[\frac{1}{R}\left(\frac{\partial\phi}{\partial s}\right)_0 - \left(\frac{\partial^2\phi}{\partial n\partial s}\right)_0\right] + \cdots\,, \tag{51b}$$

$$-\frac{\partial\phi}{\partial n} = -\left(\frac{\partial\phi}{\partial n}\right)_0 - \epsilon n_1\left(\frac{\partial^2\phi}{\partial n^2}\right)_0 - \cdots\,, \tag{51c}$$

where the subscript zero denotes that the partial derivatives are to be evaluated at $(s, 0)$.

We introduce also the perturbation series (note the dependence on n_1 rather than on n)

$$u_s = u_{s0}(s) + \epsilon u_{s1}(s, n_1) + \cdots\,, \qquad u_n = \epsilon u_{n1}(s, n_1) + \cdots\,, \qquad \sigma = \epsilon^{-1}\sigma_{-1}(s, n_1) + \cdots\,. \tag{52}$$

To lowest order in ϵ, we now obtain for equations (48):[4]

$$\frac{\partial}{\partial s}(\sigma_{-1}u_{s0}) + \frac{\partial}{\partial n_1}(\sigma_{-1}u_{n1}) = 0\,, \tag{53a}$$

$$u_{s0}\frac{du_{s0}}{ds} = -\left(\frac{\partial\phi}{\partial s}\right)_0\,, \tag{53b}$$

$$-\frac{u_{s0}^2}{R} = -\left(\frac{\partial\phi}{\partial n}\right)_0 - 2u_{s0}\,. \tag{53c}$$

Equations (53b) and (53c) involve only functions of s and are equivalent to the orbit equations (32a) and (32b); e.g., the integration of equation (53b) leads to Jacobi's integral. Equation (53a) can be solved for σ_{-1} once we know $u_{n1}(s, n_1)$. To obtain equations which determine $u_{n1}(s, n_1)$, we consider the momentum equations for the order ϵ^1 terms. After some cancellation allowed by the zero-order equations (53), we obtain

$$u_{s0}\frac{\partial u_{s1}}{\partial s} + u_{s1}\frac{du_{s0}}{ds} + u_{n1}\frac{\partial u_{s1}}{\partial n_1} + \frac{u_{n1}u_{s0}}{R} = -n_1\left(\frac{\partial^2\phi}{\partial n\partial s}\right)_0 + 2u_{n1}\,, \tag{54a}$$

$$u_{s0}\frac{\partial u_{n1}}{\partial s} + u_{n1}\frac{\partial u_{n1}}{\partial n_1} + n_1\frac{u_{s0}^2}{R} - 2\frac{u_{s0}u_{s1}}{R} = -n_1\left(\frac{\partial^2\phi}{\partial n^2}\right)_0 - \frac{1}{\sigma_{-1}}\frac{\partial\sigma_{-1}}{\partial n_1} - 2u_{s1}\,. \tag{54b}$$

[4] If $(\partial\phi/\partial s)_0$ were zero, as it nearly is for orbits in the rotating disk, equations (53b) and (53c) would be equivalent to the "gradient wind approximation" of Prendergast (1960). For the stream, however, $(\partial\phi/\partial s)_0$ is far from being nearly equal to zero since the stream necessarily crosses equipotentials if it is to be accelerated.

Inspection of equations (53a), (54a), and (54b) shows that it is possible to look for solutions in which σ_{-1} is even in n_1, but u_{s1} and u_{n1} are odd. Thus, there is no correction of the trajectory for the stream center to order ϵ^1; such corrections must be $O(\epsilon^2)$ (cf. § I). To be able to match the solutions obtained in § III*c*, we try solutions in which the differential velocities are linear in n_1, and the surface density is Gaussian:

$$u_{s1} = \alpha(s)n_1 , \qquad u_{n1} = \beta(s)n_1 , \qquad \sigma_{-1} = \sigma_{-10}(s) \exp\left[-\tfrac{1}{2}\gamma(s)n_1^2\right] . \tag{55}$$

The substitution of equations (55) into equations (53a), (54a), and (54b) reduces these partial differential equations to the following set of ordinary differential equations:

$$\frac{d}{ds}(\sigma_{-10}u_{s0}) + \sigma_{-10}\beta = 0 , \qquad u_{s0}\frac{d\gamma}{ds} + 2\beta\gamma = 0 , \tag{56a}$$

$$u_{s0}\frac{d\alpha}{ds} + \frac{du_{s0}}{ds}\alpha + \left(\frac{u_{s0}}{R} + \alpha\right)\beta = -\left(\frac{\partial^2\phi}{\partial n \partial s}\right)_0 + 2\beta , \tag{56b}$$

$$u_{s0}\frac{d\beta}{ds} + \beta^2 + \frac{u_{s0}^2}{R^2} - 2\frac{u_{s0}}{R}\alpha = -\left(\frac{\partial^2\phi}{\partial n^2}\right)_0 + \gamma - 2\alpha . \tag{56c}$$

Note now that the elimination of β from equations (56a) results in a relation which can be integrated to give

$$\left(\frac{2\pi}{\gamma}\right)^{1/2}\sigma_{-10}u_{s0} = \text{constant} = 1 . \tag{57}$$

The identification of the constant as unity follows from the integral constraint (49).

We can use Bernoulli's theorem to motivate another integration. Consider the possible variation of Bernoulli's constant on *different* streamlines. In the L1 region, the variation of each term, $|\boldsymbol{u}|^2/2$, ϕ, and $\epsilon^2 \log \sigma$, is of order ϵ^2. Since Bernoulli's constant is conserved on each individual streamline leading away from the L1 region, the order ϵ^1 term in Bernoulli's integral must vanish identically for a streamline at distance $n = \epsilon n_1$ from the center of the stream in the orbit region. From the expansions (51) and (52), the coefficient for the order ϵ^1 term in Bernoulli's integral is easily seen to be

$$u_{s0}u_{s1} + n_1\left(\frac{\partial\phi}{\partial n}\right)_0 = n_1\left[u_{s0}\alpha + \left(\frac{\partial\phi}{\partial n}\right)_0\right];$$

thus, we require that the term in the square brackets vanish identically for all s. This is possible because equation (56b) can be written in the form

$$\frac{d}{ds}\left[u_{s0}\alpha + \left(\frac{\partial\phi}{\partial n}\right)_0\right] = \beta\left(2 - \frac{u_{s0}}{R} - \alpha\right) , \tag{58}$$

and by equation (53c), the requirement $\alpha = -u_{s0}^{-1}(\partial\phi/\partial n)_0$ is equivalent to the requirement

$$\alpha = 2 - u_{s0}/R . \tag{59}$$

This provides the requisite integration of equation (56b).

An alternative physical interpretation can be attached to equation (59). The absolute vorticity is the quantity

$$\boldsymbol{\omega} = 2\boldsymbol{e}_z + \nabla \times \boldsymbol{u} . \tag{60}$$

According to Kelvin's circulation theorem, the number of absolute vortex lines which thread an element of area remains constant if we follow the fluid motion. On the surface of the contact component the z-component of the absolute vorticity is very nearly equal to 2 because the relative vorticity, $\nabla \times \boldsymbol{u}$, is small by the assumption that the star rotates nearly synchronously. On the other hand, by moving to the orbit region from the surface layer, the element of area has expanded typically by a factor ϵ^{-2}; thus, the absolute vorticity must vanish to order ϵ^2. A straightforward calculation shows $|\boldsymbol{\omega}|$ in the orbit region to be $2 - \alpha - u_{s0}/R$ to zeroth order, and equation (59) is simply the expression that this quantity is zero.

The linear velocity profile across the stream, $\partial u_s/\partial n = \alpha(s)$, clearly cannot extend infinitely far in the n-direction. Our asymptotic solution (55) must break down for values of n comparable to R. To be able to obtain the flow for $n_1 = O(\epsilon^{-1})$, it is necessary to solve for the flow in the transonic shell. Fortunately, for $\epsilon \ll 1$, there is very little matter far from the center of the gas stream, and, apart from the disk, we are justified in ignoring the dynamic role of the material outside of the main stream.

With the derivation of expression (59) for α, the stream spreading problem reduces to the solution of the coupled set consisting of the second of equations (56a) and equation (56c). Their integration must be performed numerically

with the "initial values" for β and γ to be supplied by asymptotic matching at L1. In the limit $s \to 0$, $x \to s \cos(\theta_s) - n \sin(\theta_s)$, $y \to s \sin(\theta_s) + n \cos(\theta_s)$, and

$$u_{s0} \to \lambda_1 s\,, \qquad \phi \to -\tfrac{3}{2}A(s\cos\theta_s - n\sin\theta_s)^2 + \tfrac{1}{2}(A-1)(s^2+n^2)\,. \tag{61}$$

Thus, equations (53b) and (53c) become

$$\lambda_1{}^2 = 3A\cos^2\theta_s - (A-1)\,, \qquad \lambda_1 = -\tfrac{3}{2}A\cos\theta_s\sin\theta_s\,, \tag{62}$$

which are equivalent to equations (23a) and (23b). The linear acceleration of the stream now implies, through equation (57), that the density of the center of the stream decreases as $1/s$ as the stream flows away from L1, in agreement with the asymptotic behavior implied by equation (21). The substitution of equations (59), (61), and (62) into equations (56a) and (56c) gives

$$\beta = 0\,, \qquad \gamma = \lambda_1{}^2 - A + 2 \equiv \lambda_3{}^2 \qquad \text{as} \qquad s \to 0\,. \tag{63}$$

The second relation is equivalent to equation (25a) if we identify $\gamma = \Theta''(\theta_s)$ with $U(\theta_s) = \lambda_1$. The differential velocities implied by equation (59) and the first of relations (63) are consistent with those implied by equations (25b) and (25c) if we take into account the differences between the coordinates (s, n) and (r, θ).

With the starting values (63), we can integrate equations (56a) and (56c) numerically to obtain β and γ as functions of s. In practice, analytic series solutions valid in the neighborhood of $s = 0$ are required to provide correct

TABLE 3

STREAM CHARACTERISTICS

Location	s	X	Y	u_X	u_Y	R	$\epsilon^2\rho$ $(n = z = 0)$	α	β	$(2\pi/\gamma)^{1/2}$	$(2\pi)^{1/2}/\omega_z$
					$M_D/M_C = 0.0667$						
L1.....	0.000	0.686	0.000	0.000	0.000	−1.28	...	2.00	0.00	0.985	1.01
$\frac{1}{2}s(\varpi_d)$....	0.124	0.804	−0.039	0.474	−0.106	−0.455	6.05	3.06	− 2.24	0.677	0.505
ϖ_d.....	0.249	0.926	−0.039	1.42	0.591	−0.089	27.2	19.4	− 8.52	0.291	0.082
ϖ_{min}.....	0.296	0.959	−0.007	0.660	2.08	−0.041	79.2	55.2	−69.9	0.170	0.034
					$M_D/M_C = 0.5000$						
L1.....	0.000	0.237	0.000	0.000	0.00	−6.53	...	2.00	0.00	0.880	0.898
$\frac{1}{2}s(\varpi_d)$....	0.210	0.438	−0.062	0.865	−0.196	−0.876	3.33	3.01	− 1.83	0.694	0.487
ϖ_d.....	0.420	0.645	−0.065	2.57	0.986	−0.153	13.9	20.1	− 9.16	0.336	0.078
ϖ_{min}.....	0.501	0.703	−0.013	1.30	3.69	−0.069	37.9	58.3	−68.1	0.206	0.033
					$M_D/M_C = 1.6667$						
L1.....	0.000	−0.177	0.000	0.000	0.000	8.95	...	2.00	0.00	0.875	0.892
$\frac{1}{2}s(\varpi_d)$....	0.265	0.074	−0.083	1.02	−0.266	−1.18	2.24	2.89	− 1.27	0.785	0.539
ϖ_d.....	0.530	0.335	−0.098	2.84	0.824	−0.230	7.18	14.8	− 7.67	0.431	0.109
ϖ_{min}.....	0.654	0.430	−0.024	1.70	3.84	−0.108	19.	40.8	−44.	0.28	0.047
					$M_D/M_C = 4.5000$						
L1.....	0.000	−0.467	0.000	0.000	0.000	2.78	...	2.00	0.00	0.915	0.934
$\frac{1}{2}s(\varpi_d)$....	0.298	−0.188	−0.105	0.996	−0.319	−1.45	1.58	2.72	− 0.694	0.937	0.645
ϖ_d.....	0.597	0.106	−0.144	2.55	0.393	−0.343	3.52	9.53	− 5.06	0.607	0.182
ϖ_{min}.....	0.788	0.264	−0.050	1.91	3.15	−0.169	8.27	23.8	−20.7	0.396	0.083
					$M_D/M_C = 7.0000$						
L1.....	0.000	−0.563	0.000	0.000	0.000	2.02	...	2.00	0.00	0.940	0.961
$\frac{1}{2}s(\varpi_d)$....	0.308	−0.278	−0.116	0.949	−0.339	−1.60	1.35	2.63	− 0.477	1.03	0.711
ϖ_d.....	0.615	0.023	−0.169	2.34	0.185	−0.410	2.52	7.71	− 3.85	0.719	0.235
ϖ_{min}.....	0.846	0.223	−0.070	1.95	2.73	−0.207	5.44	18.2	−12.9	0.489	0.112
					$M_D/M_C = 15.0000$						
L1.....	0.000	−0.686	0.000	0.000	0.000	1.28	...	2.00	0.00	0.985	1.01
$\frac{1}{2}s(\varpi_d)$....	0.313	−0.402	−0.131	0.828	−0.358	−1.91	1.07	2.46	− 1.30	1.22	0.849
ϖ_d.....	0.626	−0.102	−0.214	1.91	−0.123	−0.551	1.46	5.48	− 2.07	0.985	0.363
ϖ_{min}.....	0.936	0.184	−0.121	1.94	1.96	−0.291	2.66	11.5	− 4.34	0.742	0.184

starting conditions because $s = 0$ is a regular singular point of the differential equations (56). We do not present details here but merely tabulate some numerical results in Table 3. In these calculations, we also integrated equation (56b) numerically and used equation (59) as a check on the accuracy of the results.

The rapid increase of the stream velocity, $u_s = (u_X^2 + u_Y^2)^{1/2}$, from L1 leads initially to a rapid decrease of the central stream density, $\rho(n = z = 0)$. Later, the stretching of the fluid elements in the s-direction is more than offset by the vertical compression associated with the decrease in the z-thickness, $\epsilon(2\pi)^{1/2}/\omega_z$. Apart from these effects, the salient qualitative features are the constancy of the stream width, $\epsilon(2\pi/\gamma)^{1/2}$, on the straight portion of its path and the narrowing of the stream as it curves toward the detached component. The behavior in the n-direction near L1 results because the differential inertial and gravitational forces act, like the banks of a river, to confine the stream against the spreading tendency produced by the internal pressure. For example, the shear across the stream is such that the inside edge of the stream moves faster than the outside edge. The differential Coriolis forces always act, therefore, to throttle the stream toward its center. As the stream approaches $\varpi_{\min}$, the differential inertial effects narrow the stream while the differential gravity acts oppositely. The pressure forces play a minor role here because the sound travel time across the width of the stream is relatively long compared with the orbit time characterizing the local flow.

A detailed comparison of our results with those of Prendergast and Taam (1974) would show fairly good agreement for the trajectory of the stream center but not for its width. We do not find this discrepancy surprising because we believe the spreading obtained in their calculations is due more to the artificial diffusion associated with finite mesh spacing than with the effects of pressure.

Our stream-spreading calculations were generally terminated when the stream reaches $\varpi_{\min}$. If the detached component is smaller than $\varpi_{\min}$, we have already argued that the steady-state resolution of the subsequent stream-stream interactions would be to produce a disk of orbiting material whose edge radius ϖ_d is larger than $\varpi_{\min}$.

An interesting question arises if the radius of the detached component is larger than $\varpi_{\min}$ but smaller than ϖ_d. Would the outermost parts of the stream still miss striking the star, and would the subsequent cumulative interactions with the incident stream still end up producing a (weak) disk? Another interesting scenario arises if the detached component expands because of core evolution beyond $\varpi_{\min}$ after a disk has already been established. Definitive answers to these problems await an honest calculation of the internal dynamics of an accretion disk.

V. THE SURFACE LAYER OF THE CONTACT COMPONENT

We finish our formal analysis of the gas dynamics of semidetached binaries with a brief discussion of the flow in the surface layers of the contact component. We remark at the outset that the surface layers discussed here need not coincide with the optical atmosphere of the star since the depth over which the optical depth at visual wavelengths reaches unity is not *a priori* related to the depth over which appreciable mass flow occurs.

For the latter problem, it is clearly advantageous to adopt the Roche coordinates invented jointly by Prendergast (1960) and Kopal (1972). Remembering that $\boldsymbol{e}_z = e_{z\xi}\boldsymbol{e}_\xi + e_{z\zeta}\boldsymbol{e}_\zeta$ in the notation adopted in § II, we can write the fluid equations (1) and (2) in the form[5]

$$\frac{\partial}{\partial\xi}(h_\eta h_\zeta \rho u_\xi) + \frac{\partial}{\partial\eta}(h_\zeta h_\xi \rho u_\eta) + \frac{\partial}{\partial\zeta}(h_\xi h_\eta \rho u_\zeta) = 0\,, \tag{64a}$$

$$\frac{u_\xi}{h_\xi}\frac{\partial u_\xi}{\partial\xi} + \frac{u_\eta}{h_\xi h_\eta}\frac{\partial}{\partial\eta}(h_\xi u_\xi) + \frac{u_\zeta}{h_\zeta h_\xi}\frac{\partial}{\partial\zeta}(h_\xi u_\xi) - \frac{u_\eta^2}{h_\xi h_\eta}\frac{\partial h_\eta}{\partial\xi} - \frac{u_\zeta^2}{h_\zeta h_\xi}\frac{\partial h_\zeta}{\partial\xi} = -\frac{1}{h_\xi\rho}\frac{\partial}{\partial\xi}(\epsilon^2\rho) - \frac{1}{h_\xi} + 2e_{z\xi}u_\eta\,, \tag{64b}$$

$$\frac{u_\xi}{h_\xi h_\eta}\frac{\partial}{\partial\xi}(h_\eta u_\eta) + \frac{u_\eta}{h_\eta}\frac{\partial u_\eta}{\partial\eta} + \frac{u_\zeta}{h_\eta h_\zeta}\frac{\partial}{\partial\zeta}(h_\eta u_\eta) - \frac{u_\zeta^2}{h_\eta h_\zeta}\frac{\partial h_\zeta}{\partial\eta} - \frac{u_\xi^2}{h_\xi h_\eta}\frac{\partial h_\xi}{\partial\eta} = -\frac{1}{h_\eta\rho}\frac{\partial}{\partial\eta}(\epsilon^2\rho) + 2(e_{z\xi}u_\zeta - e_{z\zeta}u_\xi)\,, \tag{64c}$$

$$\frac{u_\xi}{h_\zeta h_\xi}\frac{\partial}{\partial\xi}(h_\zeta u_\zeta) + \frac{u_\eta}{h_\eta h_\zeta}\frac{\partial}{\partial\eta}(h_\zeta u_\zeta) + \frac{u_\zeta}{h_\zeta}\frac{\partial u_\zeta}{\partial\zeta} - \frac{u_\xi^2}{h_\zeta h_\xi}\frac{\partial h_\xi}{\partial\zeta} - \frac{u_\eta^2}{h_\eta h_\zeta}\frac{\partial h_\eta}{\partial\zeta} = -\frac{1}{h_\zeta\rho}\frac{\partial}{\partial\zeta}(\epsilon^2\rho) - 2e_{z\xi}u_\eta\,. \tag{64d}$$

We have written the equations (64) in a form which does not assume that ϵ^2 is a constant because the temperature structure may have important hydrodynamic effects in the surface layers, and it should properly be determined, in principle, by the simultaneous solution of the equation of heat transfer.

The above equations are also to be solved subject to the integral constraint that the outward mass flux integrated over any equipotential surface which encloses only the contact component be unity, i.e.,

$$\iint_{\xi<0} \rho u_\xi h_\eta h_\zeta d\eta d\zeta = 1\,. \tag{65}$$

In the deep interior of the contact component ($|\xi|$ of order unity), the outward mass flux must be nearly uniform on the entire equipotential surface. The density ρ is of order ϵ^{-3} in an ϵ neighborhood of L1, but it is of order

[5] The fluid equations written down by Kopal (1972) are missing the Coriolis terms.

ϵ^{-4} in the surface layers (where $|\xi|$ is of order ϵ^2). Since u_ξ is of order ϵ in an ϵ neighborhood of L1 and since it can be at most ϵ^4 elsewhere in the surface layer, the contribution to the integrated outward mass flux (65) from the L1 region is at least comparable to that from the rest of the surface layer. In fact, as we go higher and higher up in the atmosphere, more and more of the outward mass flux must be carried by the wind at L1. This can be consistent with the equation of continuity (64a) only if the outward mass flux is converted more and more into horizontal currents in the surface layer. Such horizontal currents must coexist with horizontal pressure gradients, and the relation between the two is given to lowest order by the "astrostrophic approximation,"

$$\rho u_\zeta = (2e_{z\xi})^{-1} \frac{1}{h_\eta} \frac{\partial}{\partial \eta} (\epsilon^2 \rho) , \qquad \rho u_\eta = -(2e_{z\xi})^{-1} \frac{1}{h_\zeta} \frac{\partial}{\partial \zeta} (\epsilon^2 \rho) , \tag{66}$$

whose rigorous derivation from equations (64c) and (64d) can be justified by introducing perturbational techniques like those considered in the previous sections. We shall forgo such a discussion, and merely remark here that equation (66) implies that the horizontal velocities are of order ϵ^2 if the logarithmic gradients of density and temperature in the horizontal directions are of order unity. In this situation, $u_\xi \ll u_\eta$ or u_ζ, and the streamlines lie nearly on equipotential surfaces.

Equations (66) can be written in vector form with advantage:

$$\rho \boldsymbol{u}_\perp = \frac{\boldsymbol{e}_\xi}{2e_{z\xi}} \times \nabla_\perp (\epsilon^2 \rho) \equiv \frac{\boldsymbol{e}_\xi}{2e_{z\xi}} \times \left(\frac{\boldsymbol{e}_\eta}{h_\eta} \frac{\partial}{\partial \eta} + \frac{\boldsymbol{e}_\zeta}{h_\zeta} \frac{\partial}{\partial \zeta} \right) (\epsilon^2 \rho) , \tag{67}$$

which shows explicitly that the horizontal component of the fluid velocity is parallel to isobars in the astrostrophic approximation. Like the large-scale circulation patterns in the atmosphere and oceans of the Earth, the flow does not simply proceed from high pressures to low, but is directed around the contours of equal pressure. In the northern hemi-lobe, the flow proceeds by keeping the region of high (low) pressure to the right (left); in the southern hemi-lobe, by keeping high (low) pressure to the left (right). (Eq. [67] breaks down near the equator where $e_{z\xi}$ vanishes.) On a given equipotential surface, we expect the pressure to be largest at the poles (for the same reason that meridional circulation obtains in rotating stars) and smallest at L1 (because of the mass-loss flow); therefore equation (67) implies that the excess circulation should be counter to the sense of the orbit rotation. This expectation has been incorporated schematically in Figure 3.

In the vertical direction, the pressure scale-height is of order ϵ^2, and hydrostatic equilibrium holds with good approximation since the velocities are all small:

$$\epsilon^2 \rho = p(\eta, \zeta) \exp \left(- \int_0^\xi \epsilon^{-2} d\xi \right) . \tag{68}$$

The substitution of equations (68) and (66) into equation (64a) leaves us with a single equation which relates the unknown functions p, ϵ^2, and u_ξ. Clearly, even with ϵ^2 known from a simultaneous solution of the heat transfer problem, we cannot determine the horizontal variation of the pressure without knowing the vertical velocity u_ξ. The determination of u_ξ, consistent with appropriate boundary conditions deep inside the star and zero mass flux very high up, requires a higher-order calculation than the one discussed here. We leave such a calculation for future investigations; for the present, we merely remark that the result should lead to a slow drift of the matter from the poles to the equator as matter is slowly pushed outward by the evolutionary expansion. On each equipotential surface, the flow may be astrostrophic, i.e., parallel to isobars, but a net transfer of matter within the entire surface layer to the equator is possible because the quantity

$$\frac{d}{d\zeta} \left(\int_{-\pi}^{+\pi} d\eta \int_{\text{surface layer}} \rho u_\zeta h_\xi h_\eta d\xi \right) = \int_{-\pi}^{+\pi} (\rho u_\xi)_{\text{bottom of surface layer}} h_\zeta h_\eta d\eta \tag{69}$$

must be positive if there is an outward flux of matter at the bottom of the surface layer.

Another effect which reinforces the concept that there must be a slow drift of matter from the poles to the equator, and thence to L1, occurs if the envelope of the contact component is convective. In this case, the effective frictional drag exerted on the upper layers by the lower layers must produce the "Ekman effect" (Ekman 1922) where the induced secondary flow corresponds to a drift across isobars from high pressures to low. Indeed, we suspect that all nonastrostrophic effects lead to this pattern of behavior for the secondary flow. Once the matter reaches the equator, it can flow more or less directly to the L1 region.

An interesting problem revolves around the question of whether this flow is unstable to oscillations as are the zonal winds in the atmosphere (Kuo 1949, 1951). Such oscillations, if present, could manifest themselves in intermittent effects in the stream.

VI. DISCUSSION

Clearly, the theoretical development presented in the previous sections can be subjected to a number of geometric and kinematic observational tests. We shall comment on detailed comparisons with individual binary systems

elsewhere, but a thorough discussion of such matters is well beyond the scope of the present paper. We content ourselves, instead, by commenting on two general points of contact with observations.

1. The theory provides a natural explanation for two of the three classical components of circumstellar matter: stream and disk, but not "cloud" (Batten 1973). Narrow streams are present in all systems where ϵ is small (§ IV), but disks can arise only if the radius of the detached component is smaller than ϖ_d tabulated in Table 2. These disks rotate in a direct sense with respect to the orbital motion, in apparent agreement with the observations (Struve 1950). The density and velocity fields of the stream is calculable in dimensional form from the results derived in § IV provided that d, Ω, and $\dot{M}$ are known along with ϵ and M_D/M_C. These seem generally to be consistent with values deduced from observations.

2. Huang and Struve (1956) have shown that the relation between emission-line velocity and orbital period found by Struve for Algol-type systems (see Struve 1950, p. 191),

$$V_{\rm em}{}^3 P \approx \text{constant}\,, \tag{70}$$

can be understood theoretically if the quantity (in the notation of the present paper),

$$M_D f\,, \qquad \text{where} \qquad f \equiv \left(\frac{M_D}{M_C + M_D}\right)^{1/2} \varpi_d{}^{-3/2} = \mu^{1/2} \varpi_d{}^{-3/2}\,, \tag{71}$$

does not vary appreciably from one eclipsing system to another.[6] The detached components of Algol-type systems are primarily main-sequence stars of spectral type between A5 and B5 for which M_D does not vary greatly. According to our analysis, the quantity f depends only on the mass ratio M_D/M_C. Figure 5 shows that $f(M_D/M_C)$ is relatively insensitive to the ratio M_D/M_C. Thus, Struve's relation (70) is easily understood on the approximate basis that the product $M_D f$ is likely to vary even less than either of its two individual factors when $M_D > M_C$.

To generalize the discussion for other types of systems, we expand the discussion of Huang and Struve to note that a measurement of the velocity of the disk edge, V_d, in a frame of reference fixed instantaneously at rest with respect to the detached component, would determine the mass M_D of the detached component as

$$M_D = \frac{V_d{}^3 P}{2\pi G f(M_D/M_C)}\,. \tag{72}$$

In principle, V_d could be determined by measuring, at the appropriate phase, the fluid velocity of the "hot spot" produced by the impact of the stream with the disk. The mass ratio M_D/M_C can be determined from a measurement of various eclipse durations; fortunately, Figure 5 shows that even a crude estimate of M_D/M_C serves to fix $f(M_D/M_C)$ fairly precisely if $M_D < M_C$. This method allows, therefore, an accurate dynamical determination of the mass of a small detached component predicated only on the assumptions that ϵ is small, that the contact component rotates synchronously, and that the disk edge is much denser than the stream. This method is potentially of great value in the determination of the masses of invisible companions such as neutron stars or black holes.

We wish to thank C. C. Lin for some illuminating discussions concerning turbulence, transonic flow, and the multiple-scale approximation technique. We are grateful to Harold Weaver who stimulated and guided our initial interest in the problem of semidetached binaries; to Lawrence Anderson, Telemachos Mouschovias, Jon Arons, and Peter Biermann who provided helpful criticisms and theoretical discussions while this work was in progress; and to Len Kuhi and David Koo who informed us on various observational matters. We wish also to acknowledge

[6] The small adjustment to the analysis of Huang and Struve required by eq. (41) does not appreciably change the conclusions given here.

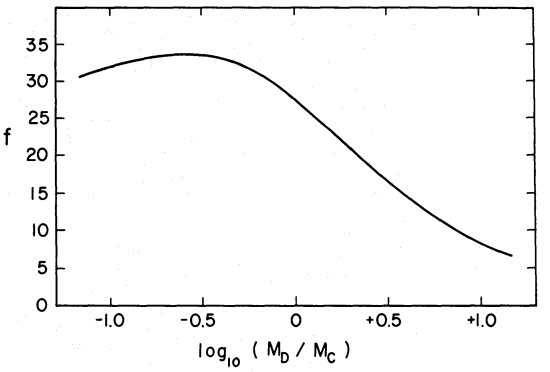

FIG. 5.—The function $f(M_D/M_C)$ plotted against $\log_{10}(M_D/M_C)$

Kevin Prendergast and Ronald Taam for kindly sending us a preprint of their work in advance of publication. The numerical calculations for this paper were performed on the IBM 1620 computer in the Berkeley Physics Department.

REFERENCES

Arons, J. 1973, *Ap. J.*, **184**, 539.
Batten, A. H. 1973, *Binary and Multiple Systems of Stars* (Oxford: Pergamon Press).
Biermann, P. 1971, *Astr. and Ap.*, **10**, 205.
Chandrasekhar, S. 1961, *Hydrodynamic and Hydromagnetic Stability* (Oxford: Clarendon Press).
Cole, J. D. 1968, *Perturbation Methods in Applied Mathematics* (Waltham: Blaisdell).
Ekman, W. 1922, *Dynamische Gesetzeden Meersstromungen* (Innsbrucker Vortage).
Faulkner, J. 1972, *Ap. J.* (*Letters*), **170**, L99.
Garabedian, P. R. 1964, *Partial Differential Equations* (New York: Wiley).
Giacconi, R. 1974, in *IAU Symposium No. 64*, ed. C. Dewitt-Morette (Dordrecht: Reidel), p. 147.
Holton, J. R. 1972, *An Introduction to Dynamic Meteorology* (New York: Academic Press).
Huang, S. S. 1967, *Ap. J.*, **148**, 793.
Huang, S. S., and Struve, O. 1956, *A.J.*, **61**, 300.
Kitamaru, K. 1970, *Ap. and Space Sci.*, **7**, 272.
Kopal, Z. 1959, *Close Binary Systems* (New York: Wiley).
———. 1972, *Adv. Astr. and Ap.*, **9**, 1.
Kraft, R. P. 1963, *Adv. Astr. and Ap.*, **2**, 43.
Kraft, R. P., Matthews, J., and Greenstein, J. L. 1962, *Ap. J.*, **136**, 312.
Kruszewski, A. 1966, *Adv. Astr. and Ap.*, **4**, 233.
———. 1967, *Acta Astr.*, **17**, 297.
Kuiper, G. P. 1941, *Ap. J.*, **93**, 133.
Kuo, H. L. 1949, *J. Met.*, **10**, 235.
———. 1951, *Tellus*, **3**, 268.
Lamb, F. K., Pethick, C. J., and Pines, D. 1973, *Ap. J.*, **184**, 271.
Lin, C. C. 1955, *The Theory of Hydrodynamic Stability* (Cambridge: Cambridge University Press).
Morton, D. C. 1960, *Ap. J.*, **132**, 146.
Moulton, F. R. 1914, *An Introduction to Celestial Mechanics* (New York: Macmillan).
Nariai, K. 1967, *Pub. Astr. Soc. Japan*, **19**, 564.
Ostriker, J. P., and Davidson, K. 1973, in *IAU Symposium No. 55*, ed. H. Bradt and R. Giacconi (Dordrecht: Reidel), p. 143.
Paczynski, B. 1971, *Ann. Rev. Astr. and Ap.*, **9**, 183.
Parker, E. N. 1963, *Interplanetary Dynamical Processes* (New York: Interscience).
Prendergast, K. H. 1960, *Ap. J.*, **132**, 162.
Prendergast, K. H., and Burbidge, G. R. 1968, *Ap. J.* (*Letters*), **151**, L83.
Prendergast, K. H., and Taam, R. E. 1974, *Ap. J.*, **189**, 125.
Pringle, J. E., and Rees, M. J. 1972, *Astr. and Ap.*, **21**, 1.
Roberts, W. W., and Shu, F. H. 1972, *Ap. Letters*, **12**, 49.
Salpeter, E. E. 1973, in *IAU Symp. No. 55*, ed. H. Bradt and R. Giacconi (Dordrecht: Reidel), p. 135.
Shu, F. H. 1974, *Astr. and Ap.*, **33**, 55.
Strittmatter, P. A., Scott, J., Whelan, J., Wickramasinghe, E. T., and Woolf, N. J. 1973, *Astr. and Ap.*, **25**, 275.
Strömgren, E. 1935, *Bull. Astr. Paris*, **9**, 87.
Struve, O. 1950, *Stellar Evolution* (Princeton: Princeton University Press).
Szebehely, V. 1967, *Theory of Orbits—The Restricted Problem of Three Bodies* (New York: Academic Press).
Van Dyke, M. D. 1964, *Perturbation Methods in Fluid Mechanics* (New York: Academic Press).
Warner, B., and Peters, W. L. 1972, *M.N.R.A.S.*, **160**, 15.
Zel'dovich, Ya. B., and Novikov, I. D. 1964, *Soviet Phys. Doklady*, **9**, 246.

Note added in proof.—After this paper was accepted for publication, it came to our attention via John Faulkner that Brian Flannery had also discovered the error in the paper by Warner and Peters (see § IV*c*). Flannery's (1975, *M.N.R.A.S.*, **170**, 325) results are in excellent agreement with ours (cf., e.g., the entries for unit mass ratio in his Table 1 and our Table 2). The slight remaining differences are attributable primarily to Flannery's having adopted somewhat arbitrary ejection conditions at L1.

STEPHEN H. LUBOW: Physics Department, University of California, Berkeley, CA 94720

FRANK H. SHU: Astronomy Department, University of California, Berkeley, CA 94720